Available online at www.sciencedirect.com
ScienceDirect
International Journal of Multiphase Flow 33 (2007) 766–788
International Journal of Multiphase Flow
www.elsevier.com/locate/ijmulflow

A hybrid Eulerian–Lagrangian method to simulate the dispersed phase in turbulent gas-particle flows

Xavier Pialat [a,b,*], Olivier Simonin [b], Philippe Villedieu [a]

[a] DMAE, ONERA-CERT, 2 avenue Edouard Belin, 31500 Toulouse, France
[b] IMFT, UMR CNRS-INPT-UPS 5502, Allée du Professeur Camille Soula, 31400 Toulouse, France

Received 21 June 2006; received in revised form 19 February 2007

Abstract

This paper presents a methodology to combine stochastic Lagrangian approach and continuum model to simulate the dispersed phase in gas-particle turbulent flows using that both approaches are based on the same Boltzmann-like kinetic equation governing the joint fluid-particle probability density function (pdf). The proposed hybrid method is based on the separate application of each approach in two adjacent domains and their coupling at the interface via flux boundary conditions. Validation of the method is carried out for non-colliding solid particles suspended in homogeneous turbulent shear flow without two-way coupling.

Pacs: 47.11.+j; 47.55.Kf

Keywords: Particle-laden flows; Pdf approach; Langevin equation; Lagrangian particle tracking; Continuum model; Half-flux coupling

1. Introduction

Gas-particle flows are found in a very wide range of applications, from industrial (fluidized bed, turbomachines) to natural (pollutant dispersion, sand transport) processes. This diversity has led to an extended zoology of formalisms to model such flows (Mashayek and Pandya, 2003). It is thus unsurprising that numerical treatments vary from one problem to another. Actually, when dealing numerically with gas-particle flows it is usual to choose from a variety of approaches the one that better suits the problem. The choice extends from direct numerical simulation/discrete particle system (DNS/DPS) models to two-fluid models, each formalism accounting for different levels of description. Naturally, the more accurate the description, the more expensive the simulations.

* Corresponding author. Address: DMAE, ONERA-CERT, 2 avenue Edouard Belin, 31500 Toulouse, France. Tel.: +33 562252525x2440.
E-mail addresses: pialat@imft.fr (X. Pialat), simonin@imft.fr (O. Simonin), philippe.villedieu@onera.fr (P. Villedieu).

0301-9322/$ - see front matter
doi:10.1016/j.ijmultiphaseflow.2007.02.003

The dispersed phase Lagrangian approaches, from deterministic Lagrangian (DPS) coupled with a DNS for the fluid phase (Squires and Eaton, 1990, 1991; Elghobashi and Truesdell, 1992; Sundaram and Collins, 1997) to stochastic Lagrangian (Gosman and Ioannides, 1981; Sommerfeld and Zivkovic, 1992) coupled with RANS equations for the fluid phase, simulate the behavior of particles following their trajectories. These approaches take place at a mesoscopic level, allowing "direct" accounting in the simulations of physical phenomena like rebound, coalescence, break-up, etc. (Sommerfeld, 1999). However, the simulations are limited by the amount of tracked particles, which make deterministic Lagrangian approaches not suited for spatially complex and/or extended flows. The stochastic Lagrangian approaches, which aim to approximate a probability density function (pdf) which contains the one-point statistical information on the system (Mc Innes and Bracco, 1992; Sommerfeld et al., 1993), are a fair attempt to reduce this drawback, but nevertheless inherit the limitations imposed by computer resources.

In such situations, one would prefer to use coarser descriptions like continuum models (also called Eulerian). The two phases are then treated as separate interpenetrating continua, and mean equations are solved for both phases and coupled through interphase transfer terms (Elghobashi and Abou-Arab, 1983; Chen and Wood, 1986). Among these Eulerian approaches, pdf based methods consider a few of low order moments of the pdf, limiting the accuracy of such approaches (Derevich and Zaichik, 1988; Reeks, 1991; Simonin, 1991). This choice is motivated by computational efficiency as it is well known that good accuracy can be reached at low computational costs by such methods where the flow can be considered near equilibrium. It is however not fully justified to use closure laws in non-equilibrium zones occurring, for example, when the particle relaxation time and particle–particle collision time are locally larger than the mean and turbulent gas flow characteristic times (He and Simonin, 1993; Wang et al., 1998; Sakiz and Simonin, 1999). In addition, specific problems such as particle–wall interactions or jets-crossing are known to be very difficult to handle in an Eulerian framework.

When comparing the approaches (both Lagrangian and Eulerian) derived from the pdf point of view, the first remark is that they are consistent with each other, which is made especially clear by the kinetic derivation of the Eulerian equations (Reeks, 1991; Pope, 1994; Simonin, 1996). Another important remark is their complementarity: whereas pdf Eulerian approaches are really computationally efficient but do not allow to precisely account for complex phenomena, the stochastic Lagrangian approaches allow these accounts as a counterpart of expensive simulations. The drawbacks of one family is precisely the advantages of the other one.

A very similar complementarity is also encountered in rarefied gas dynamics as the Navier–Stokes equations and Monte-Carlo methods rely on the same Boltzmann kinetic equation. The computation of atmosphere re-entry vehicles flows can then be resolved by coupling kinetic and fluid equations in separate domains (Schneider, 1996; Le Tallec and Mallinger, 1997; Schwartzentruber and Boyd, 2006). This type of method, referred in the following as hybrid method, is also developed in micro- and nano-fluid flows where molecular dynamics approaches are coupled with continuum fluid dynamics approaches (O'Connell and Thompson, 1995; Nie et al., 2004; Werder et al., 2005). Another example of multi-level description based on a pdf point of view, although the domains are not separated, can be found in the prediction of reactive turbulent flows (Muradoglu et al., 1999).

Like in the above-mentioned flows, the physical phenomena that the continuum approach fail to account for typically occur near the walls or in particle-rarefied zones. By using a continuum approach in the core of the flow and a particle one in the non-equilibrium regions (to account for Knudsen effects, rough wall bouncing, deposition, splashing ...), a hybrid simulation would use the continuum approach wherever possible (thus saving computer costs) while allowing to incorporate the preceding physical phenomena with the particle approach where it is needed.

This paper is thus dedicated to the development of a hybrid method coupling a particle (stochastic Lagrangian) and a continuum (Eulerian moment method) approach to simulate the dispersed phase in turbulent gas–solid flows. The spatial domain is split into two regions: Ω_{lag} where the particulate flow is simulated in the Lagrangian framework and Ω_{eul} where the flow is simulated in the Eulerian framework. The spatial decomposition presented in this paper concerns non-overlapping regions presented in Fig. 1. We limit the study to the case of monodispersed solid particles suspended in air (Simonin et al., 1995). For the sake of simplicity, but without loss of generality, we will neglect two-way coupling and particle–particle collisions.

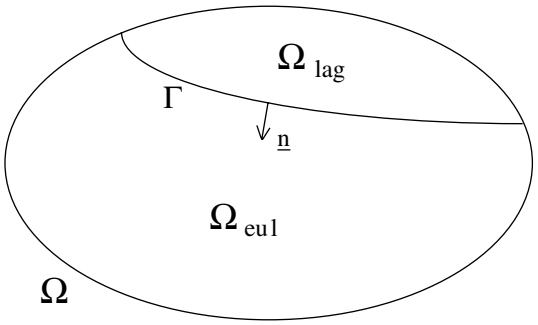

Fig. 1. Partitioning of the computational domain in Eulerian (Ω_{eul}) and Lagrangian (Ω_{lag}) domains.

The article is structured as follow. First, both the stochastic Lagrangian and Eulerian approaches are presented in the scope of a joint fluid-particle pdf approach of the dispersed phase. A coupling methodology associated to this new hybrid method is then proposed, based on a coupling by half-fluxes and associated with the hypothesis of a joint fluid-particle pdf of the Gaussian form. The consistency of the two approaches (Eulerian and stochastic Lagrangian) is then proved in a simplified case to ensure that the coupling methodology proposed is relevant in turbulent gas-particle flows. Finally, the application of the full hybrid method is carried out in the case of a homogeneous turbulent shear flow with non-overlapping domains.

2. Statistical description of gas–solid flows

Inspired by the statistical modeling of mono-atomic gases (Grad, 1949), early formalisms in gas–solid flows have represented the dispersed phase in terms of probabilities. The particle phase is described thanks to a probability density function (pdf) $f_p(\underline{c}_p, \underline{x}, t)$. This description was extended by several authors (Buyevich, 1971; Reeks, 1980; Derevich and Zaichik, 1988) to account for the modulation of the particle motion by the fluid turbulence. In particular, Simonin (1996) added to the relevant variables the fluid velocity seen by the particles. Following, a joint fluid-particle pdf f_{fp} was introduced: $f_{fp}(\underline{c}_f, \underline{c}_p, \underline{x}, t)\mathrm{d}\underline{c}_f\,\mathrm{d}\underline{c}_p\,\mathrm{d}\underline{x}$ is the probable number of particles at time t, with center of mass $\underline{x}_p \in [\underline{x}, \underline{x} + \mathrm{d}\underline{x}]$, velocity $\underline{u}_p \in [\underline{c}_p, \underline{c}_p + \mathrm{d}\underline{c}_p]$, and viewing a fluid velocity $\tilde{\underline{u}}_f \in [\underline{c}_f, \underline{c}_f + \mathrm{d}\underline{c}_f]$. It can be shown that f_{fp} obeys a Boltzmann-like equation:

$$\frac{\partial f_{fp}}{\partial t} + \frac{\partial}{\partial x_i}[c_{p,i} f_{fp}] = -\frac{\partial}{\partial c_{p,i}}\left[\left\langle \frac{\mathrm{d}u_{p,i}}{\mathrm{d}t}\middle| \underline{c}_f, \underline{c}_p, \underline{x}\right\rangle f_{fp}\right] - \frac{\partial}{\partial c_{f,i}}\left[\left\langle \frac{\mathrm{d}\tilde{u}_{f,i}}{\mathrm{d}t}\middle| \underline{c}_f, \underline{c}_p, \underline{x}\right\rangle f_{fp}\right] + \left(\frac{\partial f_{fp}}{\partial t}\right)_{coll}. \tag{1}$$

The first term on the right-hand side involves the operator $\left\langle \frac{\mathrm{d}u_{p,i}}{\mathrm{d}t}\middle| \underline{c}_f, \underline{c}_p, \underline{x}\right\rangle$ which accounts for the influence of the particle acceleration on f_{fp}. The second term involves the operator representing the influence of the fluid velocity acceleration along particle paths. Both of these terms involve a conditional statistical average $\langle \cdot \mid \underline{c}_f, \underline{c}_p, \underline{x}\rangle$ conditioned by the position, velocity and seen fluid velocity of any particle: $\underline{x}_p = \underline{x}, \underline{u}_p = \underline{c}_p$ and $\tilde{\underline{u}}_f = \underline{c}_f$.

Finally, the last term accounts for the modification of f_{fp} by inter-particle collisions and can be modeled using an extended kinetic theory formalism which takes into account the correlations stemming from the turbulence (Simonin et al., 2002). The main effect, in turbulent shear flow, is a reduction of the anisotropy of the particle fluctuating motion. However, the collisions do not influence the numerical treatment of the direct coupling between Lagrangian and Eulerian approaches and then will be omitted in this work.

The statistical description of the gas–solid flow is then complete when models for the particle acceleration and fluid velocity acceleration along the particle path are chosen. These models, which will be used by both the Lagrangian and Eulerian approaches, are described below.

2.1. Particle acceleration

Our study considers spherical solid particles with diameter d_p comparable to the Kolmogorov length scale of the fluid η_K and high density (ρ) ratio: $\rho_p \gg p_f$ (subscript f refers to the fluid and p for the particles). In such

flows the particle response time τ_p is much larger than the Kolmogorov time scale $\tau_K : \tau_p \gg \tau_K$. In the case of non-settling particles (gravity is neglected) the main force that influence the particle motion is then the drag force $\underline{F}_d$, which is acting at the center of mass (Kim et al., 1998). With $\underline{u}_p$ the particle translation velocity and $\underline{\tilde{u}}_f$ the fluid velocity seen by the particle, the evolution equation for the particle velocity reads:

$$\frac{\mathrm{d}u_{p,i}}{\mathrm{d}t} = \frac{F_{d,i}}{m_p} = -\frac{u_{p,i} - \tilde{u}_{f,i}}{\tau_p}, \tag{2}$$

where τ_p is the particle relaxation time that stems from the drag:

$$\tau_p(|\underline{u}_p - \underline{\tilde{u}}_f|) = \frac{4}{3}\frac{\rho_p}{\rho_f}\frac{d_p}{C_D|\underline{u}_p - \underline{\tilde{u}}_f|}. \tag{3}$$

C_D is the drag coefficient, given by Schiller and Nauman (1935) as:

$$C_D = \frac{24}{Re_p}(1 + 0.15Re_p^{0.687}), \tag{4}$$

where Re_p is the particle Reynolds number (ν) denotes the kinematic viscosity):

$$Re_p = \frac{d_p|\underline{u}_p - \underline{\tilde{u}}_f|}{\nu_f}. \tag{5}$$

2.2. Fluid velocity acceleration along particle paths

The Lagrangian modeling of the fluid velocity along trajectories was thoroughly studied in single phase flows by Pope (1985,1994). This approach was extended to turbulent gas-particle flows by Simonin et al. (1993) to account for the inertia of the particles (and thus relative velocity). They proposed the following Langevin equation for the fluid velocity along the particle path (assuming summation over repeated indices):

$$\mathrm{d}\tilde{u}_{f,i} = -\left[\frac{1}{\rho_f}\frac{\partial P_f}{\partial x_i} - \nu_f\nabla^2 U_{f,i}\right]\mathrm{d}t + (u_{p,k} - \tilde{u}_{f,k})\frac{\partial U_{f,i}}{\partial x_k}\,\mathrm{d}t + G_{fp,ik}(\tilde{u}_{f,k} - U_{f,k})\,\mathrm{d}t + H_{fp}\delta W_{fp,i}, \tag{6}$$

where P_f denotes the mean pressure and $\underline{U}_f$ the mean velocity of the fluid. δW_{fp} is a Wiener process, associated with the coefficient H_{fp} which is linked to the fluid turbulence statistics. In the very low inertia limit case, one has to impose $H_{fp} = \sqrt{C_0\varepsilon_f}$, with C_0 the Kolmogorov's constant ($C_0 = 2.1$), ε_f denoting the dissipation. $\underline{\underline{G}}_{fp}$ is a tensor also linked to the fluid turbulence viewed by the particles. The modeling of this tensor is prominent in the behavior of the dispersed phase. Simonin et al. (1993) proposed several models, including crossing trajectory effect induced by a mean drift between the two phases. In this study, for the sake of simplicity, a spherical form without crossing trajectory effect is assumed:

$$G_{fp,ik} = -\frac{\delta_{ik}}{\tau^t_{fp}}, \tag{7}$$

where the characteristic time scale of the "seen" fluid turbulence (eddy–particle interaction time) τ^t_{fp} is given in terms of the Lagrangian fluid turbulent characteristic time scale of the fluid τ^t_f (which is given in terms of Eulerian variables):

$$\tau^t_{fp} = \tau^t_f = \frac{1}{\beta_1}\frac{k_f}{\varepsilon_f}, \tag{8}$$

where $\beta_1 = \frac{1}{2} + \frac{3}{4}C_0$ ($\beta_1 = \frac{3}{4}C_0$ in forced homogeneous isotropic flows) and k_f is the turbulent kinetic energy.

A more practical way to deal with Eq. (6) is to introduce the fluctuation of the seen fluid velocity $\underline{u}'_f = \underline{\tilde{u}}_f - \underline{U}_f$ around the mean fluid velocity. Introducing the fluid Reynolds stresses $R_{ff,ik}$, this mean fluid velocity evolves by:

$$\frac{\partial U_{f,i}}{\partial t} + U_{f,k}\frac{\partial U_{f,i}}{\partial x_k} = -\frac{1}{\rho_f}\frac{\partial P_f}{\partial x_i} + \nu_f\nabla^2 U_{f,i} - \frac{\partial R_{ff,ik}}{\partial x_k}. \tag{9}$$

Then, using Eqs. (9) and (6) can be written:

$$\mathrm{d}u'_{\mathrm{f},i} = \frac{\partial R_{\mathrm{ff},ik}}{\partial x_k}\,\mathrm{d}t + A_{ik}u'_{\mathrm{f},k}\,\mathrm{d}t + \sqrt{C_0\varepsilon_\mathrm{f}}\delta W_{\mathrm{fp},i}, \tag{10}$$

$$A_{ik} = -\frac{\delta_{ik}}{\tau'_{\mathrm{fp}}} - \frac{\partial U_{\mathrm{f},i}}{\partial x_k}. \tag{11}$$

It should be pointed out that a basic assumption of the proposed model derivation (Simonin et al., 1993) is to insure that the second order fluid velocity correlations sampled by the particles $\widetilde{R}_{\mathrm{ff},ij}$ are equal to the fluid Reynolds stresses $R_{\mathrm{ff},ij}$:

$$\widetilde{R}_{\mathrm{ff},ij}(\underline{x},t) = R_{\mathrm{ff},ij}(\underline{x},t). \tag{12}$$

2.3. Pdf transport equation closures

Owing the closure assumptions given in the preceding paragraphs for the particle acceleration and fluid velocity acceleration along particle paths, the terms on the rhs of Eq. (1) are written:

$$\frac{\partial}{\partial c_{\mathrm{p},i}}\left[\left\langle \frac{\mathrm{d}u_{\mathrm{p},i}}{\mathrm{d}t}\,|\underline{c}_\mathrm{f},\underline{c}_\mathrm{p},\underline{x}\right\rangle f_\mathrm{fp}\right] = \frac{\partial}{\partial c_{\mathrm{p},i}}\left[-\frac{c_{\mathrm{p},i}-c_{\mathrm{f},i}}{\tau_\mathrm{p}}f_\mathrm{fp}\right], \tag{13}$$

$$\begin{aligned}\frac{\partial}{\partial c_{\mathrm{f},i}}\left[\left\langle \frac{\mathrm{d}\tilde{u}_{\mathrm{f},i}}{\mathrm{d}t}\,|\underline{c}_\mathrm{f},\underline{c}_\mathrm{p},\underline{x}\right\rangle f_\mathrm{fp}\right] &= \frac{\partial}{\partial c_{\mathrm{f},i}}\left[\left(-\frac{1}{\rho_\mathrm{f}}\frac{\partial P_\mathrm{f}}{\partial x_i} + \nu_\mathrm{f}\nabla^2 U_{\mathrm{f},i}\right)f_\mathrm{fp}\right]\\ &+ \frac{\partial}{\partial c_{\mathrm{f},i}}\left[c_{\mathrm{p},k}\frac{\partial U_{\mathrm{f},i}}{\partial x_k}f_\mathrm{fp}\right] + \frac{\partial}{\partial c_{\mathrm{f},i}}\left[A_{ik}(c_{\mathrm{f},k}-U_{\mathrm{f},k})f_\mathrm{fp}\right] - \frac{\partial^2}{\partial c_{\mathrm{f},i}\partial c_{\mathrm{f},i}}\left[\frac{1}{2}H_\mathrm{fp}^2 f_\mathrm{fp}\right].\end{aligned} \tag{14}$$

There are several ways to solve Eq. (1) supplemented with Eqs. (13) and (14), depending on the required level of description. One could choose to use a stochastic representation of Eq. (1) to compute the flow via a stochastic Lagrangian approach, which can give (in theory) any one-point moment of the dispersed phase. As said before, a few pdf moments can also be computed using Eulerian transport equations.

3. Stochastic Lagrangian approach

Although the fluid is described only in terms of the macroscopic variables k_f and τ'_{fp} (which is much cheaper than DNS or LES), the usual scales for the particle number density in gas–solid flows ($n_\mathrm{p} \propto 10^5/\mathrm{cm}^3$) require the use of non-deterministic techniques to make Lagrangian simulations more efficient. For that reason researchers have extensively used the statistical representation of the dispersed phase since Gosman and Ioannides (1981). This statistical representation allows to work with a limited number of "numerical particles" (also called parcels) representing a set of real particles. Each numerical particle is affected with a "weight" κ, κ being the number of real particles represented by a numerical one. From a mathematical point of view, the pdf f_fp is approximated by a sum of Dirac masses:

$$f_\mathrm{fp}(\underline{c}_\mathrm{p},\underline{c}_\mathrm{f},\underline{x},t) = \sum_{m=1}^{\mathscr{N}_\mathrm{p}} \kappa_m \delta[\underline{x}-\underline{x}_\mathrm{p}^{(m)}(t)]\delta[\underline{c}_\mathrm{p}-\underline{u}_\mathrm{p}^{(m)}(t)]\cdot\delta[\underline{c}_\mathrm{f}-\underline{\tilde{u}}_\mathrm{f}^{(m)}(t)]. \tag{15}$$

$\mathscr{N}_\mathrm{p}$ is the total number of numerical particles, and can be as small as wanted (the lower limit arising from statistical considerations).

Then solving Eq. (1) (closed with (13) and (14)), in absence of collisions, is equivalent to the Lagrangian equation set based on (2) and (10). Each numerical particle variables $(\underline{x}_\mathrm{p},\underline{u}_\mathrm{p},\underline{u}'_\mathrm{f})$ obey the following equations:

$$\frac{\mathrm{d}x_{\mathrm{p},i}^{(m)}}{\mathrm{d}t} = u_{\mathrm{p},i}^{(m)}, \tag{16}$$

$$\frac{\mathrm{d}\underline{u}_{\mathrm{p},i}^{(m)}}{\mathrm{d}t} = -\frac{u_{\mathrm{p},i}^{(m)} - U_{\mathrm{f},i} - u_{\mathrm{f},i}^{\prime(m)}}{\tau_\mathrm{p}^{(m)}}, \tag{17}$$

$$\mathrm{d}u_{\mathrm{f},i}^{\prime(m)} = \frac{\partial R_{\mathrm{ff},ik}}{\partial x_k}\,\mathrm{d}t + A_{ik}u_{\mathrm{f},k}^{\prime(m)}\,\mathrm{d}t + H_\mathrm{fp}\delta W_{\mathrm{fp},i}^{(m)}, \tag{18}$$

where the terms $U_{f,i}$, $\frac{\partial R_{ff,it}}{\partial x_k}$, A_{ik} and H_{fp} represent the projection of the fluid variable fields at the location of the particle.

4. Eulerian approach

Eulerian variables may be obtained by statistical averages of the Lagrangian particle properties over an infinity of independent realizations of the flow. According to the definition of f_{fp}, ensemble averaging of any function of the particle and fluid "seen" velocities is equivalent to integration over the whole particle and fluid velocity-space. Then the particle Eulerian variables corresponding to the zero, first and second order moments of the particle velocity distribution are written:

$$n_p(\underline{x},t) = \int f_{fp}(\underline{c}_f,\underline{c}_p,\underline{x},t)\,\mathrm{d}\underline{c}_f\,\mathrm{d}\underline{c}_p, \tag{19}$$

$$n_p U_{p,i}(\underline{x},t) = \int c_{p,i} f_{fp}(\underline{c}_f,\underline{c}_p,\underline{x},t)\,\mathrm{d}\underline{c}_f\,\mathrm{d}\underline{c}_p, \tag{20}$$

$$n_p R_{pp,ij}(\underline{x},t) = \int (c_{p,i}-U_{p,i})(c_{p,j}-U_{p,j}) f_{fp}(\underline{c}_f,\underline{c}_p,\underline{x},t)\,\mathrm{d}\underline{c}_f\,\mathrm{d}\underline{c}_p, \tag{21}$$

where n_p is the particle mean number density, $\underline{U}_p$ is the particle mean velocity and $\underline{\underline{R}}_{pp}$ the particle kinetic stress tensor. For simplicity the field variables $(\underline{x},t)$ could later be omitted.

4.1. Particle moment equations

By integration of Eq. (1) over the possible particle and fluid velocities, the mean number density conservation equation is obtained as:

$$\frac{\partial}{\partial t}(n_p) + \frac{\partial}{\partial x_i}(n_p U_{p,i}) = 0. \tag{22}$$

To obtain the momentum balance equations, Eq. (1) $\times c_{p,i}$ is integrated over the particle and seen fluid velocity-spaces. The term stemming from the drag force is $n_p\langle F_{d,i}/m_p\rangle_p$ with $\underline{F}_d$ the drag force experienced by a single particle, and $\langle\rangle_p$ is the average operator over the particle phase. Using Eqs. (2) and (22) the momentum balance equations can be written:

$$n_p \frac{\mathrm{D}U_{p,i}}{\mathrm{D}t} = -\frac{\partial}{\partial x_k}[n_p R_{pp,ik}] + n_p\left\langle \frac{F_{d,i}}{m_p}\right\rangle p, \tag{23}$$

where $\mathrm{D}/\mathrm{D}t$ stands for the Lagrangian derivative with respect to the particle Eulerian velocity field, i.e.

$$\frac{\mathrm{D}}{\mathrm{D}t} \equiv \frac{\partial}{\partial t} + U_{p,k}\frac{\partial}{\partial x_k}. \tag{24}$$

The closure of Eq. (23) requires the knowledge of the second-order particle velocity correlation $R_{pp,ik}$. This can be achieved by using a Boussinesq or gradient hypothesis and local equilibrium assumptions (Hinze, 1972) but these approximations behave poorly as long as there exists production by mean velocity gradients and/or large anisotropy of the fluctuating motion. Separate transport equations for the particle kinetic stresses are required to predict such flows (Simonin, 1991; He and Simonin, 1993; Zaichik, 1999). These equations are obtained in the same way as (23) by integration over the velocities-space of Eq. (1) $\times c''_{p,i}c''_{p,j}(c''_{p,i} = c_{p,i} - U_{p,i})$:

$$\frac{\mathrm{D}R_{pp,ij}}{\mathrm{D}t} = \mathscr{D}_{p,ij} + \mathscr{P}_{p,ij} + \Pi_{p,ij}. \tag{25}$$

The first term on the rhs of Eq. (25) represents the transport of the kinetic stresses by the particle velocity fluctuations:

$$\mathscr{D}_{p,ij} = -\frac{1}{n_p}\frac{\partial}{\partial x_k}[n_p S_{ppp,ijk}], \tag{26}$$

where the triple particle velocity correlations $S_{ppp,ijk}$ have to be modeled.

The second term in the rhs of Eq. (25) represents the production of fluctuating motion by the mean particle velocity gradient:

$$\mathscr{P}_{\mathrm{p},ij} = -R_{\mathrm{pp},kj}\frac{\partial U_{\mathrm{p},i}}{\partial x_k} - R_{\mathrm{pp},ki}\frac{\partial U_{\mathrm{p},j}}{\partial x_k}. \tag{27}$$

The last term represents the interaction of the fluid with the particles. This term is the turbulent momentum transfer rate from the fluid turbulent motion:

$$\Pi_{\mathrm{p},ij} = \left\langle \frac{F_{\mathrm{d},i}}{m_\mathrm{p}} u''_{\mathrm{p},j} + \frac{F_{\mathrm{d},j}}{m_\mathrm{p}} u''_{\mathrm{p},i} \right\rangle_\mathrm{p}. \tag{28}$$

4.2. Additional Eulerian closure assumptions

Eqs. (22) and (25) are derived directly from the pdf Eq. (1) supplemented with (13) and (14) without any additional assumption, but form a system with several unclosed terms. On one hand, specific to velocity moment equations, interfacial transfer terms due to the drag force have to be written in terms of computed Eulerian variables. On the other hand, triple velocity correlations appear in the second order moment transport equations and represent the transport by the fluctuating velocity.

In order to simplify the closure of the interfacial transfer terms, Simonin (1991) proposed to approximate the non-linear dependance of the drag on the relative velocity:

$$\left\langle \frac{1}{\tau_\mathrm{p}}[u_{\mathrm{p},i} - \tilde{u}_{\mathrm{f},i}]\psi \right\rangle_\mathrm{p} = \frac{1}{\tau^\mathrm{F}_\mathrm{fp}}\langle [u_{\mathrm{p},i} - \tilde{u}_{\mathrm{f},i}]\psi \rangle_\mathrm{p}, \tag{29}$$

where $\tau^\mathrm{F}_\mathrm{fp}$ is given by $\tau^\mathrm{F}_\mathrm{fp} = \tau_\mathrm{p}(\langle |\underline{u}_\mathrm{p} - \underline{\tilde{u}}_\mathrm{f}| \rangle_\mathrm{p})$ and $\psi = \{1, u''_{\mathrm{p},j}\}$.

This assumption is equivalent to replace the particle acceleration term closure (13) in the pdf Eq. (1) by:

$$\frac{\partial}{\partial c_{\mathrm{p},i}}\left[\left\langle \frac{\mathrm{d}u_{\mathrm{p},i}}{\mathrm{d}t} \middle| \underline{c}_\mathrm{f}, \underline{c}_\mathrm{p}, \underline{x} \right\rangle f_\mathrm{fp} \right] = -\frac{1}{\tau^\mathrm{F}_\mathrm{fp}}\frac{\partial}{\partial c_{\mathrm{p},i}}[(c_{\mathrm{p},i} - c_{\mathrm{f},i}) f_\mathrm{fp}], \tag{30}$$

Eq. (29) is exact for very small particle Reynolds numbers $Re_\mathrm{p} \ll 1$ because τ_p is then independent of the relative velocity. For intermediate particle Reynolds number $Re_\mathrm{p} \leqslant 10$ the closure is proven to accurately model non-linear effects (Simonin et al., 1995; Wang et al., 1998). For larger particle Reynolds number, one has to rely on an expansion in term of the instantaneous relative velocity to improve the consistency between the Lagrangian and the Eulerian approaches in the treatment of the drag interaction terms (Sakiz and Simonin, 1998).

Therefore, using Eq. (29) the mean momentum transfer term is written:

$$n_\mathrm{p}\left\langle \frac{F_{\mathrm{d},i}}{m_\mathrm{p}} \right\rangle_\mathrm{p} = -\frac{n_\mathrm{p}}{\tau^\mathrm{F}_\mathrm{fp}}[U_{\mathrm{p},i} - U_{\mathrm{f},i} - V_{\mathrm{d},i}], \tag{31}$$

where the fluid-particle turbulent drift velocity $\underline{V}_\mathrm{d}$ arises from the statistical bias in the sampling of the turbulence by the particles (Simonin et al., 1993). In the frame of the joint fluid-particle approach, this velocity can be written in terms of a moment of the pdf f_fp:

$$V_{\mathrm{d},i}(\underline{x}, t) = \underline{\widetilde{U}}_{\mathrm{f},i}(\underline{x}, t) - \underline{U}_{\mathrm{f},i}(\underline{x}, t), \tag{32}$$

$$n_\mathrm{p}\underline{\widetilde{U}}_{\mathrm{f},i}(\underline{x}, t) = \int c_{\mathrm{f},i} f_\mathrm{fp}(\underline{c}_\mathrm{f}, \underline{c}_\mathrm{p}, \underline{x}, t)\, \mathrm{d}\underline{c}_\mathrm{f}\, \mathrm{d}\underline{c}_\mathrm{p}. \tag{33}$$

Thus the mean drag term depends on the mean fluid velocity sampled by the particles, which can be different for the true mean fluid velocity.

Using (29), the particle–turbulence interaction Eq. (28) is written:

$$\Pi_{\mathrm{p},ij} = -\frac{2}{\tau^\mathrm{F}_\mathrm{fp}}[R_{\mathrm{pp},ij} - \mathscr{R}_{\mathrm{fp},ij}], \tag{34}$$

where $\underline{\underline{\mathscr{R}}}_{\mathrm{fp}}$, is the symmetric fluid-particle velocity correlation tensor defined from the fluid-particle velocity correlation tensor $\underline{\underline{R}}_{\mathrm{fp}}$:

$$\mathscr{R}_{\mathrm{fp},ij} = \frac{1}{2}(R_{\mathrm{fp},ij} + R_{\mathrm{fp},ji}), \tag{35}$$

$$n_{\mathrm{p}} R_{\mathrm{fp},ij}(\underline{x},t) = \int (c_{\mathrm{f},i} - \widetilde{U}_{\mathrm{f},i})(c_{\mathrm{p},j} - U_{\mathrm{p},j}) f_{\mathrm{fp}}(\underline{c}_{\mathrm{f}}, \underline{c}_{\mathrm{p}}, \underline{x}, t)\, \mathrm{d}\underline{c}_{\mathrm{f}}\, \mathrm{d}\underline{c}_{\mathrm{p}}. \tag{36}$$

Thus the behavior of the particle kinetic stresses is influenced by the local values of the fluid-particle correlation $R_{\mathrm{fp},ij}$, the drag term leading either to production or destruction of the particle velocity fluctuations.

Similar to the approach of Hanjalic and Launder (1972), Simonin (2000) derived the triple particle velocity correlation model from the corresponding transport equation obtained from (1), (13) and (14). Neglecting the mean transport, the influence of the mean velocity gradient, and using a Gaussian approximation for the quadruple particle velocity correlations, the triple particle velocity correlations are written:

$$S_{\mathrm{ppp},ijk} = -K_{\mathrm{p},lk}\frac{\partial}{\partial x_l} R_{\mathrm{pp},ij} - K_{\mathrm{p},lj}\frac{\partial}{\partial x_l} R_{\mathrm{pp},ki} - K_{\mathrm{p},li}\frac{\partial}{\partial x_l} R_{\mathrm{pp},jk}, \tag{37}$$

$$K_{\mathrm{p},mn} = \frac{\tau^{\mathrm{F}}_{\mathrm{fp}}}{3} R_{\mathrm{pp},mn} + C_{\mathrm{s}}\beta_1 \tau^{\mathrm{t}}_{\mathrm{fp}} \mathscr{R}_{\mathrm{fp},mn}, \tag{38}$$

where $C_{\mathrm{s}} = 0.11$ is chosen to insure consistency with single-phase turbulent closure model (Hanjalic and Launder, 1972)) in the tracer limit case.

It is known that such model fails in non-equilibrium zones (Sakiz and Simonin, 1998). As the prediction of the triple particle velocity correlations is of importance in inhomogeneous flows, the accuracy of (38) is a good criterion to determine the location of the coupling interface.

4.3. Fluid-particle moment equations

According to 4.2 the final closure of the particle moment transport equations require the prediction of additional velocity moments: $V_{\mathrm{d},i}$ and $R_{\mathrm{fp},ij}$. Several attempts have been made to model these moments from the local characteristics of the fluid (Derevich and Zaichik, 1988) but it seems better to directly solve their transport equations (Simonin et al., 1993; Reeks, 2005). In the frame of a joint fluid-particle pdf approach, these equations are directly deduced from (1), (13) and (14). Therefore the governing equation of the fluid-particle turbulent drift velocity is obtained by integration of Eq. (1) $\times(c_{\mathrm{f},i} - U_{\mathrm{f},i})$ over the whole particle and fluid velocity-space:

$$\frac{\mathrm{D}V_{\mathrm{d},i}}{\mathrm{D}t} = -\frac{R_{\mathrm{fp},ik}}{n_{\mathrm{p}}}\frac{\partial n_{\mathrm{p}}}{\partial x_k} + \frac{\partial}{\partial x_k}[R_{\mathrm{ff},ik} - R_{\mathrm{fp},ik}] + A_{ik} V_{\mathrm{d},k}. \tag{39}$$

Concerning the fluid-particle velocity correlations, their governing equations are obtained through integration of Eq. (1) $\times c''_{\mathrm{f},i} c''_{\mathrm{p},j}$ (where $c''_{\mathrm{f},i} = c_{\mathrm{f},i} - \widetilde{U}_{\mathrm{f},i}$). It reads:

$$\frac{\mathrm{D}R_{\mathrm{fp},ij}}{\mathrm{D}t} = \mathscr{D}_{\mathrm{fp},ij} + \mathscr{P}_{\mathrm{fp},ij} + \Pi_{\mathrm{fp},ij} + \varepsilon_{\mathrm{fp},ij}. \tag{40}$$

The first rhs term $\mathscr{D}_{\mathrm{fp},ij}$ represents the dispersion by the particle fluctuating velocity:

$$\mathscr{D}_{\mathrm{fp},ij} = -\frac{1}{n_{\mathrm{p}}}\frac{\partial}{\partial x_k}(n_{\mathrm{p}} S_{\mathrm{fpp},ijk}). \tag{41}$$

As for the particle kinetic stress equations these terms have to be closed. These are modeled in order to obtain a Hanjalic–Launder like closure (Hanjalic and Launder, 1972) in the tracer limit case (Wang et al., 1998):

$$S_{\mathrm{fpp},ijk} = -K_{\mathrm{fp},lk}\frac{\partial}{\partial x_l} R_{\mathrm{fp},ij} - K_{\mathrm{fp},lj}\frac{\partial}{\partial x_l} R_{\mathrm{fp},ki} - K_{\mathrm{fp},li}\frac{\partial}{\partial x_l} R_{\mathrm{fp},jk}, \tag{42}$$

$$K_{\mathrm{fp},mn} = C_{\mathrm{s}}\beta_1 \tau^{\mathrm{t}}_{\mathrm{fp}} \mathscr{R}_{\mathrm{fp},mn}. \tag{43}$$

$\mathscr{P}_{\mathrm{fp},ij}$ represents the production of correlated motion by the mean velocity gradients (both particle and fluid):

$$\mathscr{P}_{\mathrm{fp},ij} = -R_{\mathrm{fp},kj}\frac{\partial U_{\mathrm{f},i}}{\partial x_k} - R_{\mathrm{pp},kj}\frac{\partial V_{\mathrm{d},i}}{\partial x_k} - R_{\mathrm{fp},ik}\frac{\partial U_{\mathrm{p},j}}{\partial x_k}. \tag{44}$$

Finally, $\Pi_{\mathrm{fp},ij}$ is the turbulent momentum transfer rate from the fluid turbulent motion to the correlated motion and is written using Eq. (29):

$$\Pi_{\mathrm{fp},ij} = -\frac{1}{\tau^{\mathrm{F}}_{\mathrm{fp}}}\left[R_{\mathrm{fp},ij} - \widetilde{R}_{\mathrm{ff},ij}\right]. \tag{45}$$

Finally, $\varepsilon_{\mathrm{fp},ij}$ is a dissipation term directly proportional to $R_{\mathrm{fp},ij}\varepsilon_{\mathrm{fp},ij} = -\frac{R_{\mathrm{fp},ij}}{\tau^{r}_{fp}}$.

5. Hybrid Eulerian–Lagrangian method

Sections 2–4 have given the general equation sets associated with stochastic Lagrangian and Eulerian approaches (reminded in Table 1) which can be solved separately in two adjacent regions Ω_{lag} and Ω_{eul} (see Fig. 1). The major problem in developing a hybrid method combining both the approaches is the exchange of information between them. Then, the following section is dedicated to the description of the coupling methodology developed at the interface of the two domains. By convention, the normal vector $\underline{n}(\underline{x})$ at the interface Γ is directed from Ω_{lag} to Ω_{eul} as in Fig. 1.

In each domain the approximated pdf $\hat{f}^{\mathrm{lag}}_{\mathrm{fp}}$ and $\hat{f}^{\mathrm{eul}}_{\mathrm{fp}}$ are estimated according to the corresponding approach. At the interface the pdf is given in the two halves of the particle velocity-space. For particles with $\underline{c}_{\mathrm{p}}\cdot\underline{n} < 0$, hence coming from the Eulerian region, the pdf is presumed according to the Eulerian moments at the interface. For particles with $\underline{c}_{\mathrm{p}}\cdot\underline{n} > 0$ the pdf is given by the Lagrangian calculation. The coupling is then enforced by the interface boundary conditions (as formulated in Le Tallec and Mallinger, 1997):

$$\hat{f}^{\mathrm{lag}}_{\mathrm{fp}}(\underline{x}_\Gamma, t) = \hat{f}^{\mathrm{eul}}_{\mathrm{fp}}(\underline{x}_\Gamma, t) \text{ for } \underline{c}_{\mathrm{p}}\cdot\underline{n} < 0, \tag{46}$$

$$\hat{f}^{\mathrm{eul}}_{\mathrm{fp}}(\underline{x}_\Gamma, t) = \hat{f}^{\mathrm{lag}}_{\mathrm{fp}}(\underline{x}_\Gamma, t) \text{ for } \underline{c}_{\mathrm{p}}\cdot\underline{n} > 0, \tag{47}$$

which represent the fact that "particles" ingoing in each domain are also "particles" outgoing from the other domain.

To implement the conditions (46) and (47) the fluxes across Γ need explicit formulations. The fluxes are divided between ingoing and outgoing half-fluxes (from the Lagrangian point of view, see Fig. 1). For any function Ψ of the particle and fluid velocities:

$$\mathscr{F}_\Gamma(\Psi, \underline{x}_\Gamma, t) = \int (\underline{c}_{\mathrm{p}}\cdot\underline{n})\Psi(\underline{c}_{\mathrm{p}}, \underline{c}_{\mathrm{f}}) f_{\mathrm{fp}}(\underline{c}_{\mathrm{f}}, \underline{c}_{\mathrm{p}}, \underline{x}_\Gamma, t)\,\mathrm{d}\underline{c}_{\mathrm{f}}\,\mathrm{d}\underline{c}_{\mathrm{p}}, \tag{48}$$

$$= \mathscr{F}^{+}_{\Gamma}(\Psi, \underline{x}_\Gamma, t) + \mathscr{F}^{-}_{\Gamma}(\Psi, \underline{x}_\Gamma, t), \tag{49}$$

Table 1
Dispersed phase equation set

Lagrangian domain Ω_{lag}	Eulerian domain Ω_{eul}
• $\frac{\mathrm{d}x^{(m)}_{\mathrm{p},i}}{\mathrm{d}t} = u^{(m)}_{\mathrm{p},i}$ • $\frac{\mathrm{d}u^{(m)}_{\mathrm{p},i}}{\mathrm{d}t} = -\frac{u^{(m)}_{\mathrm{p},i} - U_{\mathrm{f},i} - u'^{(m)}_{\mathrm{f},i}}{\tau^{(m)}_{\mathrm{p}}}$ • $\mathrm{d}u'^{(m)}_{\mathrm{f},i} = \frac{\partial R_{\mathrm{f}\,\mathrm{f},ik}}{\partial_k}\mathrm{d}t + A_{ik}u'^{(m)}_{\mathrm{f},k}\mathrm{d}t + \sqrt{C_0\varepsilon_{\mathrm{f}}}\delta W^{(m)}_{\mathrm{fp},i}$	• $\frac{\partial n_{\mathrm{p}}}{\partial t} = -\frac{\partial}{\partial x_k}(n_{\mathrm{p}}U_{\mathrm{p},k})$ • $\frac{\mathrm{D}U_{\mathrm{p},i}}{\mathrm{D}t} = -\frac{1}{\tau^{F}_{\mathrm{fp}}}[U_{\mathrm{p},k} - U_{\mathrm{f},k} - V_{\mathrm{d},k}] - \frac{1}{n_{\mathrm{p}}}\frac{\partial n_{\mathrm{p}}R_{\mathrm{pp},ik}}{\partial x_k}$ • $\frac{\mathrm{D}R_{\mathrm{pp},ij}}{\mathrm{D}t} = \mathscr{D}_{\mathrm{p},ij} + \mathscr{P}_{\mathrm{p},ij} + \Pi_{\mathrm{p},ij}$ • $\frac{\mathrm{D}V_{\mathrm{d},i}}{\mathrm{D}t} = -\frac{R_{\mathrm{fp},ik}}{n_{\mathrm{p}}}\frac{\partial n_{\mathrm{p}}}{\partial x_k} + \frac{\partial(R_{\mathrm{ff},ik} - R_{\mathrm{fp},ik})}{\partial x_k} + A_{ik}V_{\mathrm{d},k}$ • $\frac{\mathrm{D}R_{\mathrm{fp},ij}}{\mathrm{D}t} = \mathscr{D}_{\mathrm{fp},ij} + \mathscr{P}_{\mathrm{fp},ij} + \Pi_{\mathrm{fp},ij}$

where the outgoing half-flux is written:

$$\mathscr{F}_{\Gamma}^{+}(\Psi,\underline{x}_{\Gamma},t)=\int_{\underline{c}_{\mathrm{p}}\cdot\underline{n}>0}(\underline{c}_{\mathrm{p}}\cdot\underline{n})\Psi(\underline{c}_{\mathrm{p}},\underline{c}_{\mathrm{f}})f_{\mathrm{fp}}\,\mathrm{d}\underline{c}_{\mathrm{f}}\,\mathrm{d}\underline{c}_{\mathrm{p}},\tag{50}$$

and the ingoing half-flux:

$$\mathscr{F}_{\Gamma}^{-}(\Psi,\underline{x}_{\Gamma},t)=\int_{\underline{c}_{\mathrm{p}}\cdot\underline{n}<0}(\underline{c}_{\mathrm{p}}\cdot\underline{n})\Psi(\underline{c}_{\mathrm{p}},\underline{c}_{\mathrm{f}})f_{\mathrm{fp}}\,\mathrm{d}\underline{c}_{\mathrm{f}}\,\mathrm{d}\underline{c}_{\mathrm{p}}.\tag{51}$$

5.1. Boundary condition for the Lagrangian approach

The treatment of the boundary condition (46) is made through the simulation of the half-flux

$$\mathscr{F}_{\Gamma}^{-}(\Psi,\underline{x}_{\Gamma},t)=\int_{\underline{c}_{\mathrm{p}}\cdot\underline{n}<0}(\underline{c}_{\mathrm{p}}\cdot\underline{n})\Psi(\underline{c}_{\mathrm{p}},\underline{c}_{\mathrm{f}})\hat{f}_{\mathrm{fp}}^{\mathrm{eul}}\,\mathrm{d}\underline{c}_{\mathrm{f}}\,\mathrm{d}\underline{c}_{\mathrm{p}}.\tag{52}$$

The incident Eulerian pdf $\hat{f}_{\mathrm{fp}}^{\mathrm{eul}}$ is only known through a few first-order moments which are insufficient to fully characterize the pdf. Accordingly, an approximate form of the pdf has to be presumed to simulate the incident half-flux. The classical Maxwellian form cannot fit our problem due to the large anisotropy of the particle fluctuating motion observed for inertial particles suspended in turbulent shear flows. To account for this anisotropy, the best candidates are Grad's expansion (Grad, 1949) and the anisotropic Gaussian distribution proposed by Richman (1989). For large second-order moment tensor anisotropy, it is known that Grad's expansion can lead to negative non-physical values of the presumed pdf. In contrast, Richman's form seems to be a satisfactory approximation for particle pdf in shear flows (Boelle et al., 1995; Sakiz and Simonin, 1999). We now introduce an extension of this form for joint fluid-particle pdf by defining the global correlation tensor $\underline{\underline{R}}$:

$$\underline{\underline{R}}=\begin{bmatrix}\underline{\underline{R}}_{\mathrm{pp}} & \underline{\underline{\mathscr{R}}}_{\mathrm{fp}}\\ \underline{\underline{\mathscr{R}}}_{\mathrm{fp}} & \underline{\underline{R}}_{ff}\end{bmatrix},\tag{53}$$

and the global velocities $\underline{c},\underline{U}$ and $\underline{c}''$ ($^{\mathrm{t}}$ denotes transposition):

$$\underline{c}={}^{\mathrm{t}}({}^{\mathrm{t}}\underline{c}_{\mathrm{p}},{}^{\mathrm{t}}\underline{c}_{\mathrm{f}}),\ \underline{U}={}^{\mathrm{t}}({}^{\mathrm{t}}\underline{U}_{\mathrm{p}},{}^{\mathrm{t}}\widetilde{\underline{U}}_{\mathrm{f}}),\ \text{and}\ \underline{c}''=\underline{c}-\underline{U}.\tag{54}$$

With these notations, Richman's extended form for joint fluid-particle pdf reads:

$$\breve{f}_{\mathrm{fp}}(\underline{x},\underline{c},t)=\frac{n_{\mathrm{p}}(\underline{x},t)}{\sqrt{8\pi^{3}\det(\underline{\underline{R}})}}\exp\left(-\frac{1}{2}{}^{\mathrm{t}}\underline{c}''\cdot\underline{\underline{R}}^{-1}\cdot c''\right).\tag{55}$$

Unlike the Maxwellian form for monoatomic gas, there exists no mathematical argument to prove that this pdf is solution of Eq. (1) at equilibrium, but Section 7 will show that this approximation is impressively accurate up to second-order moments in homogeneous flows. Of course, third order moments of this presumed pdf being identically null, this approximation will be questionable in inhomogeneous flows.

Accordingly to Eq. (52), the pdf of the ingoing half-flux of particles can be written as:

$$g_{\mathrm{p}}^{-}(\underline{x},\underline{c},t)=|\underline{c}_{\mathrm{p}}\cdot\underline{n}|\breve{f}_{\mathrm{fp}}(\underline{x},\underline{c},t)\quad\text{for}\ \underline{c}_{\mathrm{p}}\cdot\underline{n}<0.\tag{56}$$

Indeed, $g_{\mathrm{p}}^{-}(\underline{x},\underline{c},t)\,\mathrm{d}\underline{c}\,\mathrm{d}t\,\mathrm{d}S$ is the probable number of ingoing particles with a "velocity" $\underline{u}\in[\underline{c},\underline{c}+d\underline{c}]$ passing through $\mathrm{d}S$ during $\mathrm{d}t$.

The ingoing particle flux $\delta N_{\mathrm{p}}^{-}$ across an elementary surface $\mathrm{d}S$ of Γ during $\mathrm{d}t$ associated to this half-flux can be calculated in terms of Eulerian variable values at the surface (see Section 5.2):

$$\delta N_{\mathrm{p}}^{-}=\int_{\underline{c}_{\mathrm{p}}\cdot\underline{n}<0}g_{\mathrm{p}}^{-}(\underline{x}_{\Gamma},\underline{c},t)\,\mathrm{d}\underline{c}\,\mathrm{d}S\,\mathrm{d}t,\tag{57}$$

$$=n_{\mathrm{p}}\left[(\underline{U}_{\mathrm{p}}\cdot\underline{n})g\left(\frac{\underline{U}_{\mathrm{p}}\cdot\underline{n}}{\sqrt{R_{\mathrm{pp}}^{nn}}}\right)+\sqrt{R_{\mathrm{pp}}^{nn}}h\left(\frac{\underline{U}_{\mathrm{p}}\cdot\underline{n}}{\sqrt{R_{\mathrm{pp}}^{nn}}}\right)\right]\mathrm{d}S\,\mathrm{d}t,\tag{58}$$

where R_{pp}^{nn} is the particle kinetic normal stress (in the direction of $\underline{n}$) and the functions g and h are defined by:

$$\left|\begin{array}{l} g : x \rightarrow \frac{1}{2}\left[1+\mathrm{erf}\left(\frac{x}{\sqrt{2}}\right)\right], \\ h : x \rightarrow \frac{1}{\sqrt{2\pi}}\exp\left(-\frac{x^2}{2}\right). \end{array}\right. \tag{59}$$

$\delta\mathcal{N}_p^- = \delta N_p^-/\kappa$ then gives the average number of numerical particles to inject at each time step. The effective amount is calculated by taking the integer part and comparing the fractional part to a random number to decide if another particle is injected.

The variables associated with these particles need then to respect Eq. (56) on average. The simulation of the pdf (56) is not straightforward and led us to use a rejection method (Press et al., 1997). The underlying idea is to find a simple pdf g_p^{sup} which is a majorant of the desired pdf. The phase space is then oversampled using g_p^{sup} and unfitted samples for (56) are rejected. In practical, a maximum speed of injection v_{max} is chosen according to the physics of the flow and the orientation of Γ. The majorant pdf is then taken as:

$$g_p^{sup} = v_{max}\widetilde{f}_{fp}(\underline{x},\underline{c},t). \tag{60}$$

This choice of the majorant pdf is motivated by the simple form that takes the rejection method as well as the possibility to simulate g_p^{sup} by a Choleski decomposition of $\underline{\underline{R}}$ (as $\underline{\underline{R}}$ is by definition positive symmetric). Indeed, the Gaussian form of g_p^{sup} enables to compute random variables following g_p^{sup} from a simple set of normal Gaussian independent random variables multiplied by the left part of the Choleski decomposition.

The algorithm is then sketched for each injected numerical particle as:

(1) compute random fluctuating velocities following $g_p^{sup} : (\underline{u}_p'', \underline{u}_f'')$,
(2) compare $-\underline{u}_p'' \cdot \underline{n}$ with $v_{max}z$, where z is a random number computed following a uniform law on $[0,1]$:
   (a) if $-\underline{u}_p'' \cdot \underline{n} \geqslant v_{max}z$, the particle is effectively injected in Ω_{lag} with the velocities $(\underline{U}_p + \underline{u}_p'', \widetilde{\underline{U}}_f + \underline{u}_f'')$ and advanced in time for a random duration $\delta t^* \in [0;\delta t]$,
   (b) if $-\underline{u}_p'' \cdot \underline{n} < v_{max}z$, the particle is not injected with these velocities and a new process takes place for that particle.

5.2. Boundary conditions for the Eulerian approach

Similarly with (46), the boundary condition (47) is represented via the other half of the kinetic fluxes across Γ. However, reasoning in terms of half-fluxes in the Eulerian approach is not sufficient as the physical phenomena are expressed in terms of total fluxes (see Eq. (26) for example). Moreover, usually Eulerian calculations are performed using finite volume schemes. It thus seems natural to incorporate the total fluxes into the model. To integrate the coupling in the Eulerian approach we then reconstruct the total fluxes across Γ as the sum of the ingoing and outgoing half-fluxes. The outgoing half-fluxes are given by the Lagrangian simulation while the ingoing ones need to be given. In order to avoid additional stochastic noise (which comes from the outgoing half-fluxes), these ingoing half-fluxes are explicitly calculated from the Eulerian data (assuming a joint pdf of the Richman's extended form) instead of being given by the Lagrangian simulation. These calculations are carried through successive changes of variables and give in the most general case:

$$\underline{\mathscr{F}}_\Gamma^-(n_p)\cdot\underline{n} = n_p\left[(\underline{U}_p\cdot\underline{n})g\left(\frac{\underline{U}_p\cdot\underline{n}}{\sqrt{R_{pp,nn}}}\right) + \sqrt{R_{pp,nn}}h\left(\frac{\underline{U}_p\cdot\underline{n}}{\sqrt{R_{pp,nn}}}\right)\right], \tag{61}$$

$$\underline{\mathscr{F}}_\Gamma^-(U_i)\cdot\underline{n} = U_i\underline{\mathscr{F}}_\Gamma^-(n_p)\cdot\underline{n} + n_p\Lambda_{ik}Q_{k1}R_{pp,nn}g\left(\frac{\underline{U}_p\cdot\underline{n}}{\sqrt{R_{pp,nn}}}\right), \tag{62}$$

$$\underline{\mathscr{F}}_\Gamma^-(R_{ij})\cdot\underline{n} = R_{ij}\underline{\mathscr{F}}_\Gamma^-(n_p)\cdot\underline{n} + n_p(\Lambda_{ik}Q_{k1})(\Lambda_{jl}Q_{l1})R_{pp,nn}^{3/2}h\left(\frac{\underline{U}_p\cdot\underline{n}}{\sqrt{R_{pp,nn}}}\right). \tag{63}$$

$\underline{\underline{\Lambda}}$ and $\underline{\underline{Q}}^{-1}$ are a change-of-coordinates matrices related to the diagonalization of the operator $\underline{\underline{R}}$ (see Appendix A):

$$\begin{array}{ccccc} \text{global coordinates} & \rightarrow & \Gamma \text{ coordinates} & \rightarrow & \text{velocity eigenvectors} \\ (\underline{u},\underline{v},\underline{w}) & & (\underline{u}',\underline{v}',\underline{w}') & \overset{Q^{-1}}{\rightarrow} & (\underline{u}^*,\underline{v}^*,\underline{w}^*) \\ (\underline{x},\underline{y},\underline{z}) & \overset{\Lambda}{\rightarrow} & (\underline{n},\underline{t}_1,\underline{t}_2) & & (\underline{n},\underline{t}_1,\underline{t}_2) \end{array} \tag{64}$$

These half-fluxes are then summed with the outgoing half-fluxes computed in the Lagrangian simulation. These are simply evaluated over the outgoing particles by:

$$\underline{\mathscr{F}}_\Gamma^+(\Psi)\cdot\underline{n} = \frac{\kappa}{\mathrm{d}S\,\mathrm{d}t}\sum_i \Psi_i. \tag{65}$$

The total flux $\underline{\mathscr{F}}_\Gamma(\Psi)\cdot\underline{n}$ is then simply the sum of the two previous half-fluxes, and is taken into account in the finite-volume discretization scheme at the boundary surface of the Eulerian region as following. For example with a normal vector in the direction x_k and $\underline{U}_\mathrm{p}\cdot\underline{n}=0$, the coupling is then made by linking the fluxes of the dispersion term $\mathscr{D}$ at the coupling surface to the total fluxes at this surface:

$$\langle\psi u''_{\mathrm{p},k}\rangle_\mathrm{p}|_\Gamma = \frac{1}{n_\mathrm{p}}\underline{\mathscr{F}}_\Gamma(\Psi)\cdot\underline{n}. \tag{66}$$

6. Validation test case

The validation of the proposed hybrid Eulerian–Lagrangian method with the coupling methodology presented in Section 5 is carried out for the case of an homogeneous turbulent shear flow described below. The reference results are computed from LES/DPS simulations (Laviéville, 1997) carried out with and without collisions for about 600,000 discrete particles suspended in a periodic cubic box ($L = 0.192$ m) with the physical properties resumed in Tables 2 and 3. This test-case has served in various model validations (Laviéville et al., 1997; Zaichik, 1999; Berlemont et al., 2001; Moreau et al., 2003), and the reader should refer to these references for complementary information about the corresponding results. Two types of simulation were carried with different particle density ($\rho_\mathrm{p} = 50\ \mathrm{kg\,m^{-3}}$ and $\rho_\mathrm{p} = 100\ \mathrm{kg\,m^{-3}}$). As the results give the same trend for both particle density, figures will mainly show results for the case $\rho_\mathrm{p} = 100\ \mathrm{kg\,m^{-3}}$.

The initial conditions are derived from statistically converged LES/DPS in a forced homogeneous isotropic gas-particle turbulent flow (Table 4). At time $t = 0$, the mean shear is forced for both phases with a uniform

Table 2
Particle phase

Particle properties	
Particle diameter, d_p (m)	656×10^{-6}
Particle density, ρ_p ($\mathrm{kg\,m^{-3}}$)	50, 100
Mean number density, n_p ($\mathrm{m^{-3}}$)	8.46×10^{9}

Table 3
Fluid phase

Fluid properties	
Fluid density, ρ_f ($\mathrm{kg\,m^{-3}}$)	1.17
Kinematic viscosity, ν_f ($\mathrm{m^2\,s^{-1}}$)	1.47×10^{-5}
Mean velocity gradient, S_f ($\mathrm{s^{-1}}$)	50

Table 4
Initial conditions

Homogeneous isotropic turbulence conditions	
Lagrangian time scale, $\tau^t_{\mathrm{fp}}(s)$	36.7×10^{-3}
Fluid turbulent energy, k_f ($\mathrm{m^2\,s^{-2}}$)	0.12

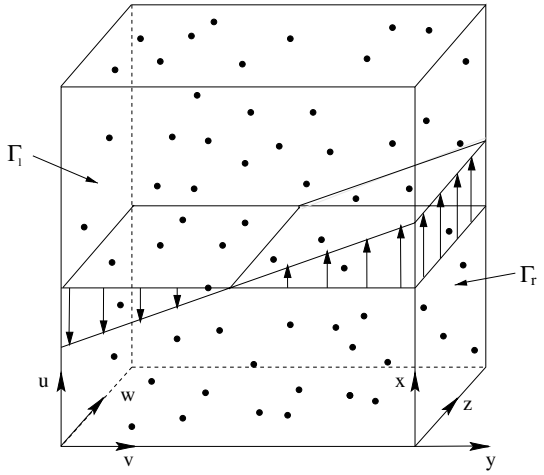

Fig. 2. Configuration of the Lagrangian box with shear flow.

fluid mean velocity gradient S_f and a particle mean velocity gradient $S_p = S_f$. For later times the simulations were run independently for the two approaches with k_f and k_f/ε_f provided by LES (with an adimensional Lagrangian time step $S_f\,dt_{lag} = 3.125 \times 10^{-3}$ and an Eulerian time-step $dt_{eul} = 5\,dt_{lag}$). The stochastic Lagrangian method was used in the periodic cubic box (Fig. 2), the periodicity inside the box referring to the fluctuating motion. Thus the particles that cross through $\Gamma_l(y = y_l)$ or $\Gamma_r(y = y_r = y_l + L)$ are re-injected through the other surface with respect to the mean velocity gradient S_p.

In a first step we verify, a minima, that we recover known results about the two approaches, in particular that the approaches can provide a good prediction of the behavior of the dispersed phase concerning the particle kinetic stress tensor (Laviéville et al., 1997; Moreau et al., 2003). Fig. 3 presents time-development of the particle kinetic stresses tensor and anisotropy tensor without collisions for the case $\rho_p = 100\ \mathrm{kg\,m^{-3}}$. Particle kinetic stress anisotropy tensor is defined as:

$$b_{pp,ij} = \frac{R_{pp,ij} - 2/3 q_p^2 \delta_{ij}}{2/3 q_p^2}. \tag{67}$$

The box is divided in 50 identical cells in the normal direction (direction of the fluid mean velocity gradient) and with almost 30000 numerical particles ($\kappa = 20$). In each cell the average over the set of particles gives the

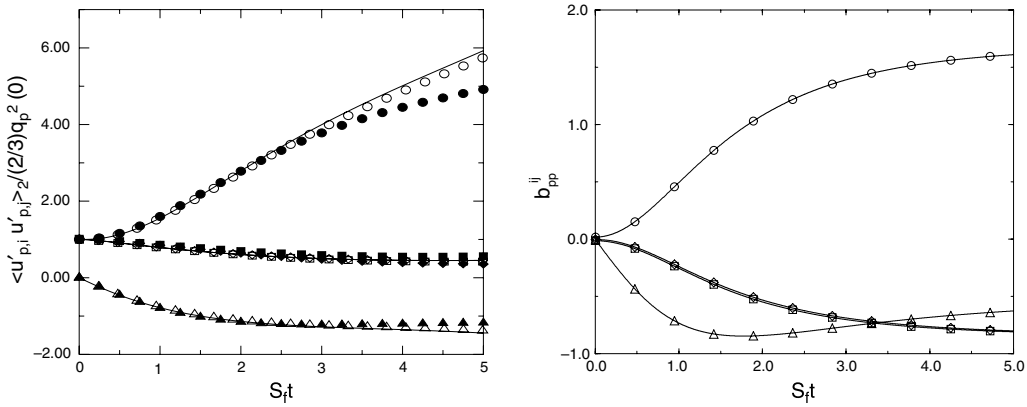

Fig. 3. On the left: time-development of the particle kinetic stresses without collisions. Comparison between stochastic Lagrangian (empty symbols) and Eulerian (lines) predictions with LES/DPS results (filled symbols). On the right: time-development of the anisotropy tensor, (○: $R_{pp,uu}, b_{pp,uu}$; □: $R_{pp,vv}, b_{pp,vv}$; ◇: $R_{pp,ww}, b_{pp,ww}$; △: $R_{pp,uv}, b_{pp,uv}$).

macroscopic quantities and the results given come from an average over the cells. As shown by Moreau et al. (2003), results from LES/DPS, stochastic Lagrangian and second-order moment simulations are in a very good agreement.

One can note that neither stochastic Lagrangian nor Eulerian approaches can reproduce the small difference in the normal and spanwise directions (square and diamonds). The particle kinetic stress in the longitudinal direction is also overestimated (Moreau et al., 2003) and present a slight difference between the two approaches. This difference between stochastic Lagrangian and Eulerian results stem from two effects. On one hand, the closure of the drag terms in the Eulerian approach induce some bias in the treatment of the interaction between the fluid and the particle phase. On the other hand, the initialization of the Eulerian simulation is made according to the steady isotropic homogeneous flow (Table 4) and thus is slightly different from the initialization of the Lagrangian simulation due to the limited number of numerical particles in the box. However, stochastic Lagrangian and Eulerian results are nearly identical, highlighting the consistency between these two approaches.

7. "A priori" half flux validation

In order to check the consistency between the chosen approaches as well as validate the calculations of our theoretical half-fluxes, we represent in Figs. 4 and 5 the mean values of the number of particle half-flux, mean particle velocity, particle–particle and particle-fluid correlation tensor components for "outgoing" particles in the case of the periodic box ($\rho_p = 100\ \mathrm{kg\,m^{-3}}$). "Outgoing" particles are the particles which overpass the left side of the box Γ_1, before being re-injected (with respect to the mean velocity gradient) on the other side of the box. Because of periodicity, they could also be considered, in terms of fluctuating motion, as ingoing particles passing through Γ_r.

The mean values over these outgoing particles can be related to the outgoing half-fluxes:

$$\langle\psi\rangle_{\underline{c}_p,\underline{n}(0,y=y_1}} \overset{def}{=} \langle\psi\rangle^- = \frac{\underline{\mathscr{F}}^-_\Gamma(\psi)\cdot\underline{n}}{\underline{\mathscr{F}}^-_\Gamma(n_p)\cdot\underline{n}} \text{ with } \underline{n} = -\underline{e}_y. \tag{68}$$

The theoretical values of these outgoing half-fluxes can be expressed by Eqs. (61)–(63), reminding that theses expressions were obtained under the hypothesis of a Gaussian form of the joint fluid-particle pdf. In that case, these ratios of half-fluxes can be expressed in terms of functions of the moments calculated in the simulations (see Appendix A):

$$\langle\psi\rangle^- = \phi_\psi(n_p, \underline{U}, \underline{\underline{R}}). \tag{69}$$

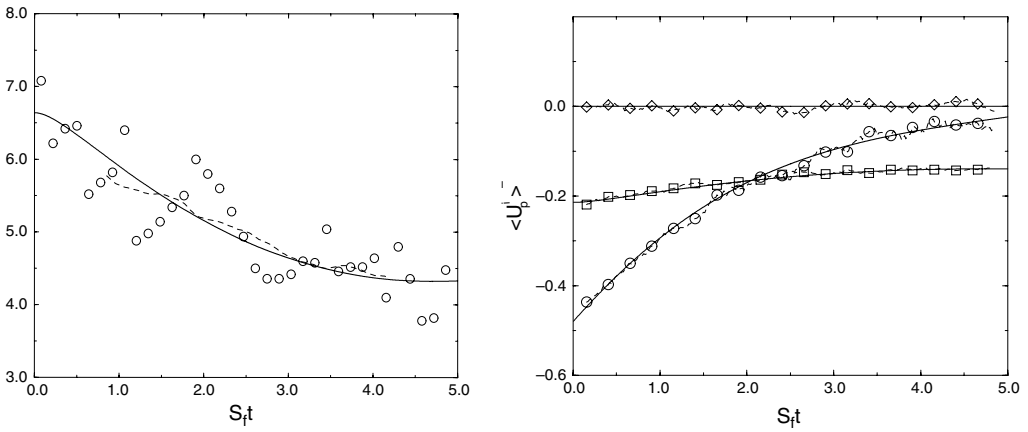

Fig. 4. Comparison between stochastic Lagrangian (empty symbols), averaged Lagrangian results (dashed line) and presumed pdf values with modeled moments (line). On the left: time-development of the number of outgoing numerical particles per time step. On the right: Time-development of the outgoing mean velocities (○: $\langle U_p\rangle^-$; □: $\langle V_p\rangle^-$; ◇: $\langle W_p\rangle^-$).

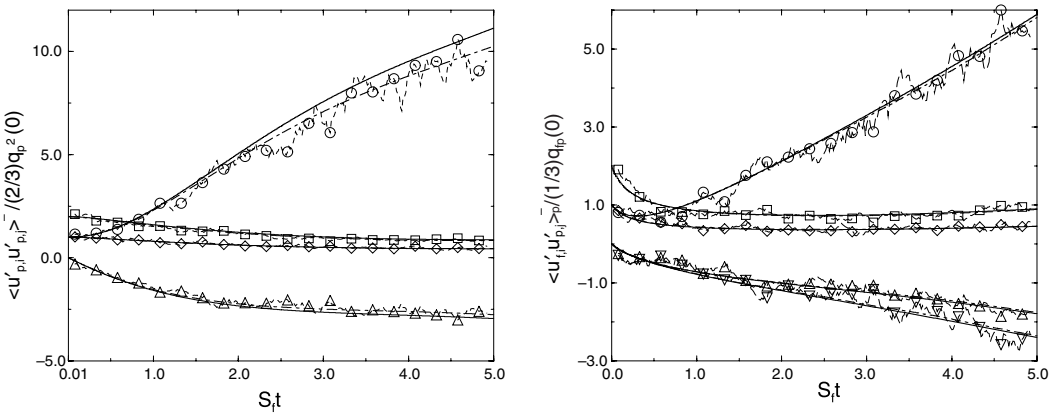

Fig. 5. Time-development of the outgoing particle-particle (left) and fluid-particle (right) velocity correlations, stochastic Lagrangian simulation (○: $\langle R_{uu}\rangle^{-}$; □: $\langle R_{vv}\rangle^{-}$; ◇: $\langle R_{ww}\rangle^{-}$; △: $\langle R_{uv}\rangle^{-}$) compared with the presumed pdf values with measured Lagrangian moments (dot-dashed lines) and calculated Eulerian moments (solid lines).

These theoretical functions will be referred in the figures as "presumed pdf values", and can be expressed either with the measured mean moments in the Lagrangian simulation or with the calculated moments in the Eulerian simulation.

We investigated the case where the side of the box has been divided by 10 and the weight by 1000 ($\kappa = 0.02$), allowing to preserve the total number of numerical particles while the number of outgoing particles is increased. In the present simulation, about 28% of the initial particles have passed through the left surface at the end of the simulation. The results for the number of outgoing numerical particles are presented averaged over 5 Lagrangian time-steps but nonetheless present a great variance due to the small number of outgoing numerical particles per time step, but an average over 100 Lagrangian time-step gives good agreement with presumed pdf values. This phenomenon is still present for other moments but are smoothed by a 10 time-step average.

The results represented in Figs. 4 and 5 show nearly exact agreement with the Gaussian-pdf half-fluxes evaluated with the measured moments, even at the beginning of the simulation at its most non-equilibrium state (in terms of unsteadiness of the anisotropy tensor $b_{\mathrm{pp},ij}$). This result should be highlighted as, by formally extending Richman's form to account for the fluid and correlated fluctuating motion (whereas previous works only account for the particle fluctuating motion), we are able to deal with a "simple" second-order joint-pdf in near-equilibrium regions of the flow. Our hybrid method thus seems appropriate as the coupled approaches are consistent one with another.

8. "One-sided" injection validation

As an intermediate validation of the proposed coupling strategy, "one-sided" simulations have been made on the basis of the preceding paragraphs. The term "one-sided" should be understood as the simulation of the boundary condition (46). We now consider the Lagrangian box with particles injected through the right surface Γ_{r} according to the presumed Gaussian pdf whose moments are given by an Eulerian calculation done simultaneously but independently. The "outgoing" particles passing through Γ_{l} are this time not re-injected through Γ_{r}. It can be convenient to take an Eulerian time step equal to several Lagrangian time steps for numerical purposes (for example when using implicit scheme in the Eulerian calculation). To account for this desired effect the particles were injected in the box during 5 Lagrangian time steps with the same presumed pdf (i.e. $m_{\mathrm{lag}} = 5$ and $m_{\mathrm{eul}} = 1$, see 9). However, the results show no significant sensibility to the time at which the Eulerian moments are taken (i.e. results are the same with Eulerian moments taken at time $i \cdot \mathrm{d}t_{\mathrm{eul}}$ or $(i+1) \cdot \mathrm{d}t_{\mathrm{eul}}$).

Fig. 6 compares the preceding periodic stochastic simulation with a onesided simulation in the time-development of the particle kinetic stresses ($\rho_{\mathrm{p}} = 100\ \mathrm{kg\,m^{-3}}$), the results being the same concerning the correlated

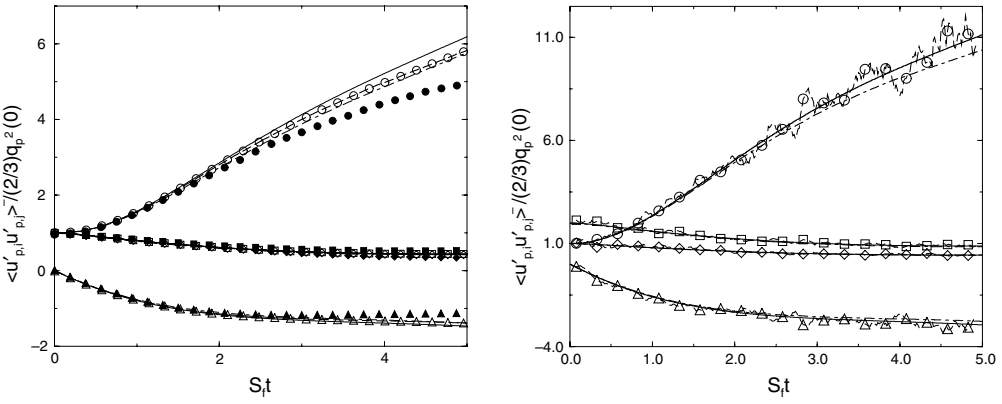

Fig. 6. Time-development of the particle kinetic stresses (left) and ingoing particle kinetic stresses (right): ○: $R_{\mathrm{pp},uu}, \langle R_{\mathrm{pp},uu}\rangle^{-}$; □: $R_{\mathrm{pp},vv}, \langle R_{\mathrm{pp},vv}\rangle^{-}$; ◇: $R_{\mathrm{pp},ww}, \langle R_{\mathrm{pp},ww}\rangle^{-}$; △: $R_{\mathrm{pp},uv}, \langle R_{\mathrm{pp},uv}\rangle^{-}$. On the left: stochastic Lagrangian with injection (empty symbols) compared to periodic stochastic Lagrangian (dot-dashed lines), Eulerian model (lines) and LES/DPS (filled symbols). On the right: stochastic Lagrangian with injection (empty symbols) compared to presumed pdf values with periodic stochastic Lagrangian moments (dot-dashed lines) and Eulerian moments (lines).

and seen fluid motion. The renewing of the particles is nearly identical as in the periodic case (28%) and the results show no significant divergence between periodic and one-sided simulations. The one-sided approach tends to slightly overestimate the particle kinetic energy due to the previously observed overestimation in the Eulerian calculation compared to the stochastic Lagrangian calculation for the case $\rho_{\mathrm{p}} = 100\ \mathrm{kg\,m^{-3}}$ (Fig. 3).

Fig. 6 also shows the mean ingoing values of the particle kinetic stress tensor simulated by the rejection method compare to the presumed pdf values (with $\underline{n} = \underline{e}_y$ and $\underline{U}_{\mathrm{p}} \cdot \underline{n} = 0$). This time the results follow tightly the Eulerian prediction, which is reassuring as these are the fluxes we intended to simulate. The stochastic noise is comparable to the periodic case which means that, despite the known great variance of rejection methods, sufficient amount of particles are injected during the 5 time steps to represent the firsts moments of the presumed pdf. These results validate our coupling methodology as well as our injection method, and it should be highlighted that the half-fluxes of the moments of order 2 are very well predicted under our hypothesis of a Gaussian joint fluid-particle pdf whereas their total fluxes are null.

9. Full hybrid Eulerian–Lagrangian method validation

The coupling methodology is applied is this section to the previous case in a fully Hybrid Eulerian–Lagrangian Method (HELM). In this precise case the total fluxes through the coupling surface should be null concerning number density and second-order moments. However, the ingoing and outgoing half-fluxes are far from null. Only their sum should be zero, which is not exactly the case in our simulations due to stochastic noise. Moreover, it is interesting to note that there still exists a momentum flux (responsible of the production of the kinetic stress R^{uv}_{pp} and R^{uv}_{fp}), thus the behavior of the method in this simplified case is a good indicator of the possibilities of the method in more complex flows.

The coupled problem is resolved with a time-marching algorithm using the following time-loop:

(1) Solve the Lagrangian equation set given in Table 1 for m_{lag} time-steps $\mathrm{d}t_{\mathrm{lag}}$ with:
   (a) regular Lagrangian boundary conditions on $\partial\Omega \cap \Omega_{\mathrm{lag}}$,
   (b) random injection of discrete particle following the presumed ingoing Eulerian pdf at the interface,
(2) Compute the outgoing Lagrangian half-fluxes $\mathscr{F}_{\Gamma}^{\mathrm{lag}+}$,
(3) Solve the Eulerian equation set given in Table 1 for m_{eul} time-steps $\mathrm{d}t_{\mathrm{eul}}$ with:
   (a) regular Eulerian boundary conditions on $\partial\Omega \cap \Omega_{\mathrm{eul}}$,
   (b) flux boundary conditions obtained from the outgoing Lagrangian half-fluxes $\mathscr{F}_{\Gamma}^{\mathrm{lag}+}$ combined with the presumed ingoing Eulerian half-fluxes $\mathscr{F}_{\Gamma}^{\mathrm{eul}-}$,

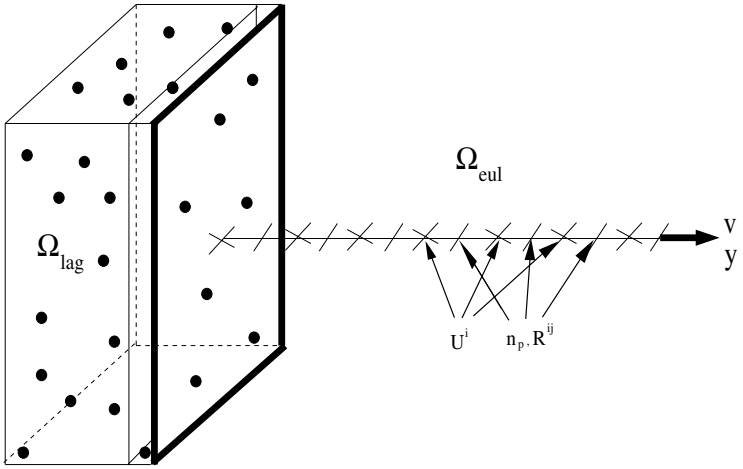

Fig. 7. Schematic description of the Lagrangian and Eulerian regions.

(4) Compute the particle and fluid velocity moments at the interface needed to presume the ingoing Eulerian pdf at the interface

where, for consistency, $m_{\text{lag}}\,\mathrm{d}t_{\text{lag}} = m_{\text{eul}}\,\mathrm{d}t_{\text{eul}}$.

As shown in Fig. 7, our Lagrangian box of Section 6 is divided into Ω_{lag} and Ω_{eul}, where Ω_{eul} is extracted from the coupling surface with the desired length such that $L_{\text{lag}} + L_{\text{eul}} = L$.

We define the volume ratio of the simulation by:

$$\eta = \frac{V_{\Omega_{\text{lag}}}}{V_{\Omega_{\text{eul}}} + V_{\Omega_{\text{lag}}}} = \frac{L_{\text{lag}}}{L}. \tag{70}$$

As this volume ratio decreases, the coupling process in the Lagrangian domain will become more and more preponderant (as the ratio $\delta\mathcal{N}_{\text{p}}^{-}/\mathcal{N}_{\text{p}}$ becomes larger). This statistical bias is not present in the Eulerian domain and therefore the influence of the coupling is constant with η. Moreover, the terms stemming from the dispersion are negligible in comparison to the drag terms Π for the kinetic stress Eq. (25).

Let us first consider the behavior of the flux splitting in the fully-coupled case ($\rho_{\text{p}} = 100\ \text{kg m}^{-3}$). Fig. 8 present the time-development of several particle moment half-fluxes and the related Eulerian flux boundary conditions, given for each Eulerian time-step (we recall that the injection of numerical particles in Ω_{lag} is constant over the 5 Lagrangian time-steps corresponding to an Eulerian one Section 8). The results for the dispersion term were filtered over a time $\Delta t = 6\,\mathrm{d}t_{\text{eul}} = 30\,\mathrm{d}t_{\text{lag}}$ such that $\Delta t S_{\text{f}} \approx 1/10$, thus representing a "mean" behavior of the flux-splitting, but at a time-scale smaller than the characteristic time-scale of behavior of the moments (which can roughly be taken as $1/S_{\text{f}}$ from Fig. 3). The results show excellent agreement with theoretical expectations despite the great variance of the stochastic Lagrangian data. This variance in the calculation is only function of the number of numerical particles passing through the coupling surface per time-step. For example, results given in Fig. 8 are obtained with approximately 30 numerical particles passing through the surface ($\mathrm{d}S = L^2$) per Eulerian time-step. This implies that with as low as 15 numerical particles passing through the surface per Eulerian time-step we can represent in "mean" the behavior of the half-fluxes and the related dispersion terms.

Fig. 9 compares the time-evolution of the kinetic stresses in the HELM simulation to LES/DPS results for the two different particle density values. Lagrangian kinetic stresses given by the HELM simulation should be understood as averaged over the whole Lagrangian region, whereas Eulerian results are given for the cell at the center of Eulerian region. The hybrid method gives satisfactory results in both cases. In particular the influence of the particle properties on kinetic stress development is well captured. Fig. 9 shows that increased inertia of the particles leads to increased anisotropy in the particle fluctuating motion, even though the fluid phase properties remain identical. The proposed methodology, even with an unsteady exchange of

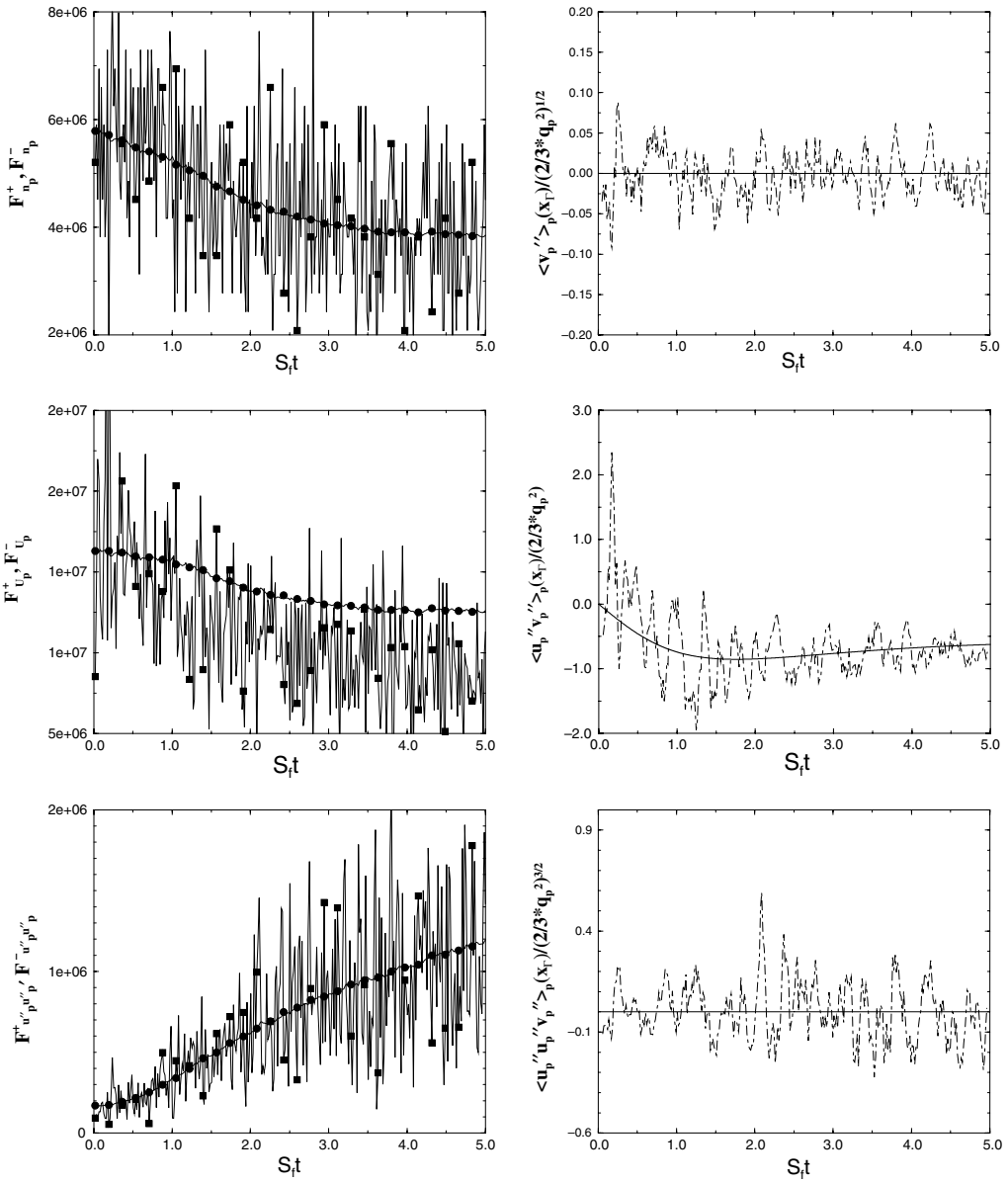

Fig. 8. Time-evolution of the fluxes for n_p, U_p and $R_{pp,uu}$. On the left: ingoing half-flux (○) and outgoing half-flux (□). On the right: value of the related Eulerian flux boundary condition averaged over a time $\Delta t = 6\,dt_{eul}$ compared with theoretical values.

information between the two approaches (Fig. 8), preserves the dynamic behavior of the two coupled approaches.

The influence of η in the stochastic Lagrangian calculation is presented in Fig. 10. It represents the time-evolution of the kinetic stresses averaged in the Lagrangian part for different η ($\rho_p = 100\,kg\,m^{-3}$). As we have kept κ as in the periodic case, the case $\eta = 0.1$ is in theory the same as Section 8, but with 10 times less particles. The average process is then not so smooth. Moreover, the coupling is done by taking into account the fluxes given by the sum of the half-fluxes of the left figures of Fig. 8 (which means not filtered over the time Δt), introducing large stochastic noise in the calculation of the flux. Nevertheless, the Hybrid Eulerian–Lagrangian Method gives nearly identical results as shown by Fig. 6.

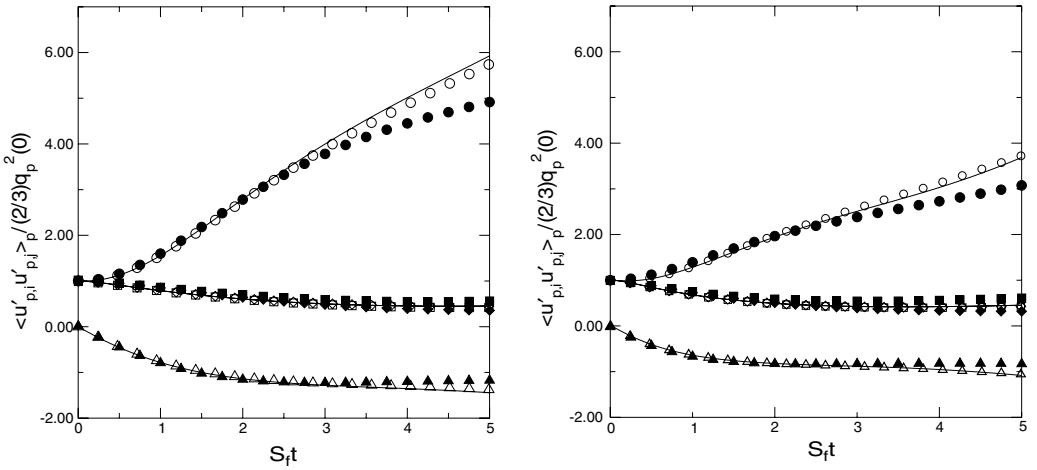

Fig. 9. Time-development of the particle kinetic stresses without collisions. Comparison between HELM results in the stochastic Lagrangian region (empty symbols) and Eulerian region (lines) with LES/DPS results (filled symbols), on the left: $\rho_p = 100$ kg m^{-3}. On the right: $\rho_p = 50$ kg m^{-3}. (○: $R_{pp,vv}$; □: $R_{pp,vv}$; ◇: $R_{pp,ww}$; △: $R_{pp,uv}$).

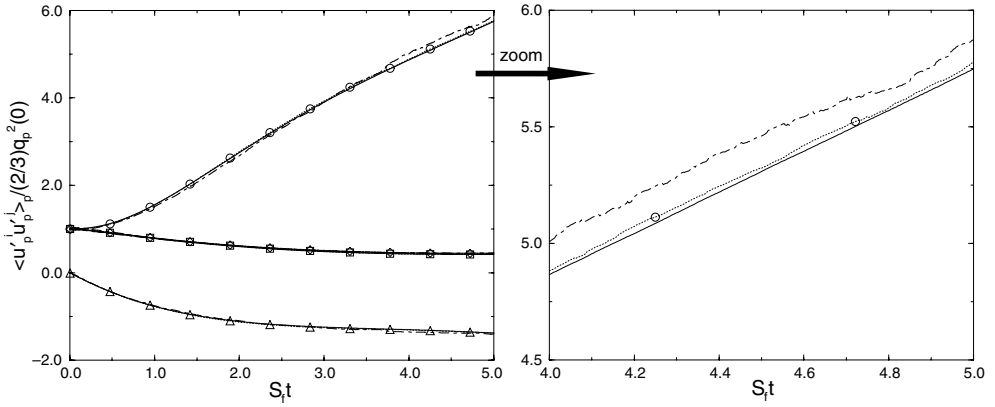

Fig. 10. Time-development of the particle kinetic stresses in Ω_{lag}. HELM, $\eta = 0.3$ (empty symbols: ○: $R_{pp,uu}, \langle R_{pp,uu}\rangle^-$; □: $R_{pp,vv}, \langle R_{pp,vv}\rangle^-$; ◇: $R_{pp,ww}, \langle R_{pp,ww}\rangle^-$; △: $R_{pp,uv}, \langle R_{pp,uv}\rangle^-$; ◇: $R_{pp,uv}, \langle R_{pp,uv}\rangle^-$) compared with HELM, $\eta = 0.1$ (dot-dashed lines) and periodic stochastic Lagrangian $\eta = 1$ (lines).

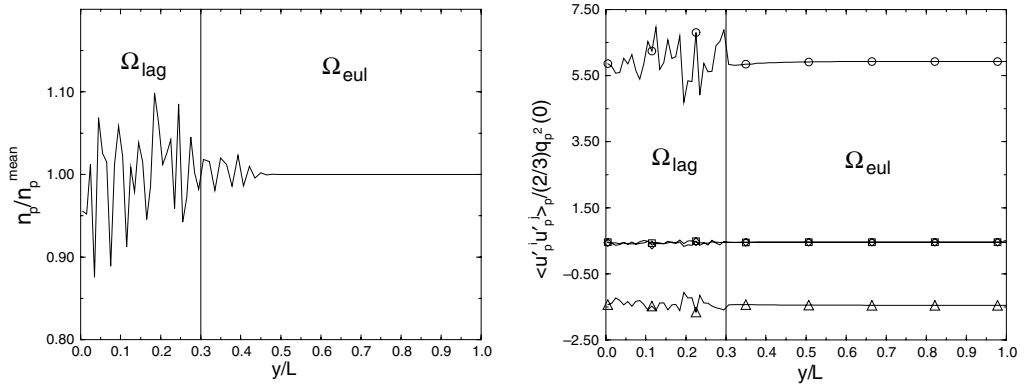

Fig. 11. Evolution in the transverse direction y at $t = 5/S_f$ of the particle density (left) and particle kinetic stresses (right) with HELM, $\eta = 0.3$. ○: $R_{pp,uu}$; □: $R_{pp,vv}$; ◇: $R_{pp,ww}$; △: $R_{pp,uv}$.

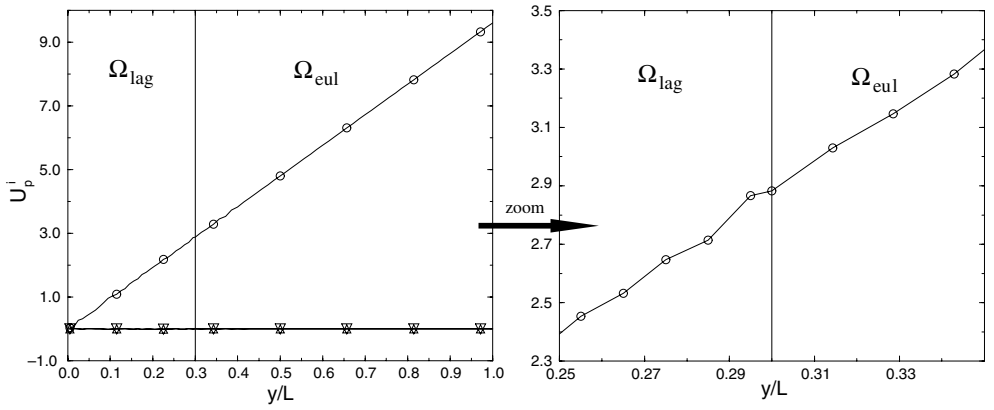

Fig. 12. Evolution in the transverse direction y at $t = 5/S_f$ of the particle mean velocity with HELM, $\eta = 0.3$. ○: U_p; △: V_p; ◇: W_p.

Fig. 11 represents the evolution in the normal direction of the particle density and kinetic stresses in the case of a volume ratio $\eta = 0.3$ at the end of the simulation ($S_f t = 5$) for the case $\rho_p = 100\ \mathrm{kg\,m^{-3}}$. These are the variables that have, in theory, null total fluxes. Fig. 8 shows that this is not perfectly true for the kinetic constraints, but the values in Ω_{lag} do not influence the values in Ω_{eul} due to the preponderance of the drag terms in the behavior of the kinetic stresses. For the mass flux, however, the flux is not entirely transparent in the Eulerian simulation. This comes from the stochastic oscillation of the total mass flux calculated in our simulation (more precisely from $\underline{\mathscr{F}}_\Gamma^+(n_p)\cdot\underline{n}$) which propagates in Ω_{eul}. However, the fluctuations in the profile of the number density in Ω_{eul} being a lot attenuated compare to those in Ω_{lag} Fig. 11 shows spectacular results in favor of the Hybrid Eulerian–Lagrangian Method.

These results are also enlightened by Figs. 8 and 12 which prove the capacity of the method to deal with non-zero fluxes as in the case of momentum fluxes. The velocity profile is very well predicted throughout the entire domain, with no discontinuities at the interface (the change of gradient is due to statistical error in the last Lagrangian cell, which can be seen with a linear regression on the left points of the zoom). This is corroborated with the excellent agreement at the interface in Fig. 11 of the kinetic stress $R_{pp,uv}$. Thus the model proves its ability to integrate non-zero fluxes, giving a good hope to deal with inhomogeneous flows as long as the coupled approaches are consistent.

10. Conclusions

A new approach to tackle turbulent gas-particle flows based on an Hybrid Eulerian–Lagrangian Method has been presented. Stochastic Lagrangian and Eulerian approaches are derived from the same joint fluid-particle pdf transport equation. Then, their complementarity is used in the frame of an hybrid method based on the separate application of each approach in two adjacent domains and their coupling at the interface via flux boundary conditions. The coupling methodology is based on a representation of the flow in the Eulerian region as a presumed joint pdf of an anisotropic Gaussian form, allowing explicit calculation of the half-fluxes and particle injection in the Lagrangian region. This methodology is then validated in the test case of turbulent homogeneous shear flow, which shows large anisotropy in the particle fluctuating motion. The half-fluxes, up to the second order, are proven to be well-predicted by a Gaussian hypothesis on the joint pdf. The method also shows excellent results in the consistency of the two coupled approaches, as well as a good behavior at the interface. All these results validate the Hybrid Eulerian–Lagrangian Method as a potential powerful tool to simulate turbulent gas-particle flows.

The work in progress is the application of the hybrid method in confined flows (particle-laden channel flows, for example) where we expect true benefits by using the moment approach in the core of the flow and the stochastic Lagrangian one in the near-wall region to account for non-equilibrium effects of the particle velocity pdf (Knudsen effects) and complex particle–wall interaction mechanisms (rough wall bouncing, deposition, splashing ...). An important issue in the development of a hybrid method that has not been discussed in

this article is the location of the coupling interface. In the test case presented here, this location is not an important matter as the continuum (Eulerian) approach is valid in the whole spatial domain. Choosing the right place to locate this interface in inhomogeneous gas–solid flow is linked to the estimation of the local level of "non-equilibrium" of the flow (Tiwari, 1998) which is related to the validity of the continuum approach. Another important issue is the validity of the presumed pdf form given at the interface by Eq. (55) in the case of inhomogeneous flows. It has been pointed out that the presumed Richman's form fails to take into account non-zero triple velocity correlations (but nonetheless can induce non-zero kinetic stress half-fluxes). As these correlations are present in inhomogeneous flows and are related to the transport of the particle kinetic stresses, an extension of this presumed form will have to be considered (based for example on a Grad expansion of the pdf). Accordingly, taking into account inhomogeneity will result in new expressions for the half-fluxes.

Appendix A. Expressions of the presumed pdf values of outgoing fluxes

For a normal vector $\underline{n} = -\underline{e}_y$, with no normal mean velocity ($\underline{U}_p \cdot \underline{n} = 0$), the theoretical values can be expressed by dividing Eqs. (62) and (63) by (61). By noting that $h\left(\frac{\underline{U}_p \cdot \underline{n}}{\sqrt{R_{pp,nn}}}\right) = \frac{1}{\sqrt{2\pi}}, g\left(\frac{\underline{U}_p \cdot \underline{n}}{\sqrt{R_{pp,nn}}}\right) = \frac{1}{2}$ and $R_{pp,nn} = R_{pp,vv}$ the explicit expressions of the mean values over the outgoing particles are:

$$\langle U_i \rangle^- = U_i + \sqrt{\frac{\pi}{2}} (\underline{\underline{\Lambda}} \cdot \underline{\underline{Q}})_{i1} \sqrt{R_{pp,vv}}, \tag{A.1}$$

$$\langle R_{ij} \rangle^- = R_{ij} + (\underline{\underline{\Lambda}} \cdot \underline{\underline{Q}})_{i1} (\underline{\underline{\Lambda}} \cdot \underline{\underline{Q}})_{j1} R_{pp,vv}. \tag{A.2}$$

In the case $\underline{n} = -\underline{y}$, a change-of-coordinates matrix $\underline{\underline{\Lambda}}$ can be chosen as:

$$\underline{\underline{\Lambda}} = \begin{pmatrix} 0 & 1 & 0 & 0 & 0 & 0 \\ -1 & 0 & 0 & 0 & 0 & 0 \\ 0 & 0 & 1 & 0 & 0 & 0 \\ 0 & 0 & 0 & 0 & 1 & 0 \\ 0 & 0 & 0 & -1 & 0 & 0 \\ 0 & 0 & 0 & 0 & 0 & 1 \end{pmatrix}. \tag{A.3}$$

We this choice of change-of-coordinates matrix we now construct the matrix $\underline{\underline{\Delta}}$ and the vector $\underline{v}'$:

$$\underline{\underline{\Delta}} = {}^t\underline{\underline{\Lambda}} \cdot \underline{\underline{R}}^{-1} \cdot \underline{\underline{\Lambda}}, \tag{A.4}$$

$$\underline{v}' = \underline{\underline{\Lambda}} \cdot \underline{v}. \tag{A.5}$$

The matrix $\underline{\underline{Q}}$ is then taken to be the change-of-coordinates matrix from the surface frame to the eigenvectors one, while $\underline{\underline{D}}$ is the diagonal matrix composed of the eigenvalues σ_i:

$$\underline{v}' = \underline{\underline{Q}} \cdot v^*, \tag{A.6}$$

$${}^t\underline{v}' \cdot \underline{\underline{\Delta}} . \underline{v}' = {}^t\underline{v}^* \cdot \underline{\underline{D}} \cdot \underline{v}^*, \tag{A.7}$$

$$\underline{\underline{D}} = \mathrm{diag}(\sigma_i). \tag{A.8}$$

References

Berlemont, A., Achim, P., Chang, Z., 2001. Lagrangian approaches for particle collisions: the colliding particle velocity correlation in the multiple particles tracking method and in the stochastic approach. Phys. Fluids 13 (10), 2496–2956.

Boelle, A., Balzer, G., Simonin, O., 1995. Second-order prediction of the particle-phase stress tensor of inelastic spheres in simple shear dense suspension. Gas-Particle Flows, ASME FED 228, 9–18.

Buyevich, Y., 1971. Statistical hydromechanics of dispersed systems Part 1: physical background and general equations. J. Fluid Mech. 49, 489–507.

Chen, C.P., Wood, P.E., 1986. Turbulence closure modeling of dilute gas-particle axisymmetric jet. AIChE J. 32 (1), 163–166.

Derevich, I., Zaichik, L., 1988. Precipitation of particles from a turbulent flow. Mekkanika Zhidkosti i Gaza 5, 96–104.

Elghobashi, S.E., Abou-Arab, T.W., 1983. A two-equation turbulence model for two-phase flows. Phys. Fluids 26 (4), 931–938.
Elghobashi, S.E., Truesdell, G.C., 1992. Direct simulation of particle dispersion in a decaying isotropic turbulence. J. Fluid Mech. 242, 655–700.
Gosman, A.D., Ioannides, E., 1981. Aspects of computer simulation of liquid-fuelled combustors. AIAA paper 81-0323.
Grad, H., 1949. On the kinetic theory of rarefied gases. Commun. Pure Appl. Math. 2, 331–407.
Hanjalic, K., Launder, B.E., 1972. A Reynolds stress model of turbulence and its application to thin shear flows. J. Fluid Mech. 52, 609–638.
He, J., Simonin, O., 1993. Non-equilibrium prediction of the particle-phase stress tensor in vertical pneumatic conveying. In: Gas–Solid Flows – 1993, ASME FED 166, pp. 253–263.
Hinze, J., 1972. Turbulent fluid and particle interaction. Prog. Heat Mass Transfer 6, 433–452.
Kim, I., Elghobashi, S., Sirignano, W.A., 1998. On the equation for spherical-particle motion: effect of Reynolds and acceleration numbers. J. Fluid Mech. 367, 221–253.
Laviéville, J., 1997. Simulations numériques et modélisation des interactions entre l'entraînement par la turbulence et les collisions interparticulaires en écoulement gas–solide. Ph.D. thesis, Université de Rouen.
Laviéville, J., Simonin, O., Berlemont, A., Chang, Z., 1997. Validation of inter-particle collision models based on large-eddy simulation in gas–solid turbulent homogeneous shear flow. In: Proceeding of the Seventh International Symposium on Gas-Particle Flows, 1997 ASME Fluids Engineering Division Summer Meeting, FEDSM97-3623.
Le Tallec, P., Mallinger, F., 1997. Coupling Boltzmann and Navier–Stokes equations by half fluxes. J. Comp. Phys. 136, 51–67.
Mashayek, F., Pandya, R.V.R., 2003. Analytical description of particle/droplet-laden turbulent flows. Prog. Energy Combust. Sci. 29, 329–378.
Mc Innes, J.M., Bracco, F.V., 1992. Stochastic particle dispersion modeling and the tracer-particle limit. Phys. Fluid A 4, 2809.
Moreau, M., Fede, P., Simonin, O., Villedieu, P., 2003. Monte-Carlo simulation of colliding particles suspended in gas–solid homogeneous turbulent shear flows. Proceedings of the Ninth International Symposium on Gas-particle Flows, Fourth ASME-JSME Joint Fluids Engineering Conference, FEDSM2003-45736.
Muradoglu, M., Jenny, P., Pope, S.B., Caughey, D.A., 1999. A consistent hybrid finite-volume/particle method for the PDF equations of turbulent re-active flows. J. Comp. Phys. 154 (2), 342–371.
Nie, X.B., Chen, S.Y., Robbins, M.O., 2004. Hybrid continuum-atomistic simulation of singular corner flow. Phys. Fluids 16 (10), 3579–3591.
O'Connell, S.T., Thompson, P.A., 1995. Molecular dynamics-continuum hybrid computations: a tool for studying complex fluid flows. Phys. Rev. E 52, R5792–R5795.
Pope, S., 1985. PDF methods for turbulent reactive flows. Prog. Energy Combust. Sci. 11, 119.
Pope, S., 1994a. Lagrangian PDF methods for turbulent flows. Annu. Rev. Fluid Mech. 1994, 23–63.
Pope, S., 1994b. On the relationship between stochastic Lagrangian models of turbulence and second-moment closures. Phys. Fluid 6, 973–985.
Press, W.H., Teukolsky, S.A., Vetterling, W.T., Flannery, B.P., 1997. Numerical Recipes in Fortran77, The Art of Scientific Computing. Cambridge University Press, Cambridge.
Reeks, M.W., 1980. Eulerian direct interaction applied to the statistical motion of particles in a turbulent fluid. J. Fluid Mech. 83, 529–546.
Reeks, M.W., 1991. On a kinetic equation for the transport of particles in turbulent flows. Phys. Fluid A 3, 446–456.
Reeks, M.W., 2005. On probability density function equations for particle dispersion in a uniform shear flow. J. Fluid Mech. 522, 263–302.
Richman, M., 1989. The source of second moment in dilute granular flows of highly inelastic spheres. J. Rheology 33 (8), 1293–1306.
Sakiz, M., Simonin, O., 1998. Continuum modeling and Lagrangian simulation of the turbulent transport of kinetic particle stresses in a vertical gas–solid channel flow. In: Proceedings of the Third International Conference on Multiphase Flows.
Sakiz, M., Simonin, O., 1999. Numerical experiments and modelling of non-equilibrium effects in dilute granular flows. In: Brun et al. (Eds.), Proceedings of the 21st International Symposium on Rarefied Gas Dynamics, 1998, vol. 1, pp. 287–294.
Schiller, L., Nauman, A., 1935. A drag coefficient correlation. VDI Zeitung 77, 318–320.
Schneider, J., 1996. Direct coupling of fluid and kinetic equations. Trans. The-oret. Stat. Phys. 25 (6).
Schwartzentruber, T.E., Boyd, I.D., 2006. A hybrid particle-continuum method applied to shock waves. J. Comp. Phys. 215 (2), 402–416.
Simonin, O., 1991. Prediction of the dispersed phase turbulence in particle-laden jets. In: Gas–Solid Flows 1991, ASME FED 121, pp. 197–206.
Simonin, O., 1996. Combustion and turbulence in two-phase flows. Von Karman Institute for Fluid Dynamics, Lecture Series 1996-02.
Simonin, O., 2000. Statistical and continuum modeling of turbulent reactive particulate flows. Part 1: Theoretical derivation of dispersed Eulerian modeling from probability density function kinetic equation. Von Karman Institute for Fluid Dynamics, Lecture Series 2000-06.
Simonin, O., Deutsch, E., Minier, J.P., 1993. Eulerian prediction of the fluid/particle correlated motion in turbulent two-phase flows. App. Sci. Res. 51, 275–283.
Simonin, O., Deutsch, E., Boivin, M., 1995. Large eddy simulation and second-moment closure model of particle fluctuating motion in two-phase turbulent shear flows. Selected Papers from the Ninth Symposium on Turbulent Shear Flows. In: Durst, F. et al. (Eds.), In: Turbulent Shear Flows, vol. 9. Springer, New York, Berlin, pp. 85–115.
Simonin, O., Février, P., Laviéville, J., 2002. On the spatial distribution of heavy-particle velocities in turbulent flows: from continuous field to particulate chaos. J. Turbulence 3 (040).
Sommerfeld, M., 1999. Modeling and calculation of turbulent gas–solid flows with the Euler/Lagrange approach. KONA (Powder and Particles) 16, 194–206.

Sommerfeld, M., Zivkovic, G., 1992. Recent advances in the numerical simulation of pneumatic conveying through pipe systems. In: Hirsch et al. (Eds.), Computational Methods in Applied Science First European Computational Fluid Dynamics Conference, Brussels, pp. 201–212.

Sommerfeld, M., Kohnen, G., Rüger, M., 1993. Some open questions and inconsistencies of Lagrangian particle dispersion models. In: Proceedings of the Ninth Symposium on Turbulent Shear Flows, Kyoto, Paper 15.1.

Squires, K.D., Eaton, J.K., 1990. Particle response and turbulence modification in isotropic turbulence. Phys. Fluids A 2 (7), 1191–1203.

Squires, K.D., Eaton, J.K., 1991. Measurements of particle dispersion obtained from direct numerical simulations of isotropic turbulence. J. Fluid Mech. 226, 1–35.

Sundaram, S., Collins, L.R., 1997. Collision statistics in an isotropic particle-laden turbulent suspension. Part 1. Direct numerical simulations. J. Fluid Mech. 335, 75–109.

Tiwari, S., 1998. Coupling of the Boltzmann and Euler equations with automatic domain decomposition. J. Comp. Phys. 144, 710–726.

Wang, Q., Squires, K.D., Simonin, O., 1998. Large eddy simulation of turbulent gas–solid flows in a vertical channel and evaluation of second-order models. Int. J. Heat Fluid Flow 19, 505–511.

Werder, T., Walther, J.H., Koumoutsakos, P., 2005. Hybrid atomistic continuum method for the simulation of dense fluid flows. J. Comp. Phys. 205, 373390.

Zaichik, L.I., 1999. A statistical model of particle transport and heat transfer in turbulent shear flows. Phys. Fluids 11 (6), 1521–1534.